FISEVIER

Contents lists available at ScienceDirect

#### Earth and Planetary Science Letters

www.elsevier.com/locate/epsl



## An early diagenetic deglacial origin for basal Ediacaran "cap dolostones"



Anne-Sofie C. Ahm <sup>a,\*</sup>, Adam C. Maloof <sup>a</sup>, Francis A. Macdonald <sup>b</sup>, Paul F. Hoffman <sup>c</sup>, Christian J. Bjerrum <sup>d</sup>, Uyanga Bold <sup>e</sup>, Catherine V. Rose <sup>f</sup>, Justin V. Strauss <sup>g</sup>, John A. Higgins <sup>a</sup>

- a Princeton University, Guyot Hall, Princeton, NJ 08540, USA
- <sup>b</sup> University of California Santa Barbara, Department of Earth Sciences, Santa Barbara, CA 93106, USA
- <sup>c</sup> University of Victoria, School of Earth and Ocean Sciences, BCV8W 2Y2, Canada
- <sup>d</sup> University of Copenhagen, Øster Voldgade 10, 1350 Copenhagen K, Denmark
- <sup>e</sup> The University of Tokyo, School of Science, Bunkyo-ku, Tokyo 113-0033, Japan
- <sup>f</sup> University of St Andrews, Irvine Building, St Andrews, United Kingdom
- g Dartmouth College, Fairchild Hall, Hanover, NH 03755, USA

#### ARTICLE INFO

# Article history: Received 12 August 2018 Received in revised form 23 October 2018 Accepted 29 October 2018 Available online 19 November 2018 Editor: L. Derry

Keywords: cap carbonate Snowball Earth Ca isotopes Mg isotopes diagenesis

#### ABSTRACT

The beginning of the Ediacaran Period ( $\sim$ 635 Ma) is marked by conspicuous dolostone units that cap Marinoan glacial deposits worldwide. The extent and sedimentary characteristics of the cap dolostones indicate that anomalous carbonate over-saturation coincided with deglacial sea-level rise and ocean warming. However, the geochemical variability within cap dolostones, both between continents, across single continental margins, and within individual stratigraphic sections has been difficult to reconcile with depositional models. Using a compilation of new calcium and magnesium isotope measurements in Marinoan cap dolostone successions worldwide, we show that the geochemical variability can be explained by early diagenetic dolomitization of aragonite along a spectrum of fluid- and sedimentbuffered conditions. Dolostones from the outer platform formed under fluid-buffered conditions, whereas dolostones on the inner platform and foreslope environment formed under sediment-buffered conditions. This spatial pattern of dolomitizing conditions is consistent with buoyant recirculation of glacial seawater within carbonate platforms driven by the deglacial sea-level rise and development of a meltwater surface ocean. Using a numerical diagenetic model to evaluate the geochemical differences between sedimentand fluid-buffered cap dolostone units, we constrain the chemical and isotopic composition of both the dolomitizing fluid (glacial seawater  $[\delta^{13}C \sim 0-2\%]$ ), the meltwater lens  $(\delta^{13}C \sim -11\%)$ , and the primary aragonite sediment ( $\delta^{13}$ C  $\sim -6$  to -3%). These model end-members do not imply that primary geochemical variability did not exist but demonstrates that it is not necessary to change the chemistry of seawater to explain the global stratigraphic variability in the geochemistry of basal Ediacaran cap dolostones. Our results provide a novel framework for understanding the geochemical variability of cap dolostone units, including large excursions in carbon isotopes, and how this variability is the product of local diagenetic processes expressed globally in continental margin environments following the last Snowball Earth.

© 2018 Elsevier B.V. All rights reserved.

#### 1. Introduction

In the Cryogenian Period ( $\sim$ 720–635 Ma), ice sheets extended to sea level in the tropics during two prolonged episodes of global glaciation (Kirschvink, 1992; Hoffman et al., 1998). The younger of these Snowball Earth events (the Marinoan) ended

E-mail address: aahm@princeton.edu (A.-S.C. Ahm).

at  $\sim$ 635 Ma and is capped by dolostone deposits that define the beginning of the Ediacaran Period (Knoll et al., 2006). These basal Ediacaran "cap dolostones" are strikingly similar across continents: they are white to buff in color with varying thickness ( $\sim$ 2–200 m) and contain unusual sedimentological features such as sheet-crack cements, tubestone stromatolites, and giant wave ripples (Kennedy, 1996; Hoffman and Schrag, 2002; Hoffman et al., 2007, 2011). Estimates from sedimentological studies, and some interpretations of the paleomagnetic data, suggest that the dolostones were deposited on timescales of  $\sim$ 10<sup>3</sup>–10<sup>5</sup> yr directly on

<sup>\*</sup> Corresponding author.

Marinoan glaciogenic deposits during the post-glacial sea-level rise (Hoffman et al., 1998; Kennedy et al., 2001; Trindade et al., 2003; Raub, 2008). In several localities, the dolostone is conformably overlain by a limestone unit that contains the post-glacial maximum flooding surface and neomorphosed aragonite and barite fans at or above the dolostone-limestone contact (Hoffman et al., 2007, 2011). Together, the cap dolostone and overlying limestone unit constitute the Marinoan "cap-carbonate sequence" (Hoffman and Schrag, 2002; Hoffman et al., 1998).

In spite of its global extent and distinct physical appearance, the cap dolostone contains a carbon isotope excursion (CIE) that is heterogeneous both in magnitude and structure on different continents. For example, in Namibia, Death Valley, and Australia, carbon isotope values ( $\delta^{13}$ C) have little stratigraphic variability within individual sections, but show a large range in  $\delta^{13}$ C across each basin ( $\sim -6$  to +2%, Hoffman, 2011; Hoffman and Macdonald, 2010; Macdonald et al., 2013b; Rose and Maloof, 2010). In contrast, individual cap dolostone sections in Mongolia, Northwest Canada, and Arctic Alaska have large stratigraphic variation in  $\delta^{13}$ C values (>3\%. Bold et al., 2016: Macdonald et al., 2009). Various hypotheses have been proposed for the origin of the cap carbonate CIE, such as turnover of a previously stratified ocean (Grotzinger and Knoll, 1995), a shutdown in biological productivity (Hoffman et al., 1998; Hoffman and Schrag, 2002), destabilization of methane hydrates following rapid warming (Kennedy et al., 2001; Jiang et al., 2003), or the combined effects of rapidly rising temperatures and CO<sub>2</sub>-drawdown by silicate weathering (Higgins and Schrag, 2003). However, none of these hypotheses can explain the range and variability in  $\delta^{13}C$  values recorded across individual continental margins and across continents.

Two models have been proposed for the origin of the Marinoan cap dolomite. Precipitation of primary dolomite is consistent with the ubiquitous dolomitic mineralogy, retention of primary fabrics (Kennedy, 1996), and the presence of coarse-grained dolomitic peloids that were reworked prior to cementation (Hoffman et al., 2011). A primary origin could imply that the cap dolostone geochemistry reflects the chemistry of the water where these sediments originally precipitated. In this model, the spatial variability in cap dolostone geochemistry would suggest either mixing of water masses across the platform (Liu et al., 2014, 2018; Yang et al., 2017) or diachronous deposition (Hoffman et al., 2007; Rose and Maloof, 2010). In the alternative model, the cap dolomite may reflect secondary dolomitization of an aragonite or calcite precursor. Due to high temperatures and pCO<sub>2</sub> levels, seawater chemistry in the glacial aftermath was more prone to primary precipitation of aragonite than dolomite (Fabre et al., 2013), and petrographic indicators (growth faults, sheet veins, and multiple generations of cements) are consistent with expansive growth of cements during early diagenetic dolomitization (Gammon et al., 2012; Gammon, 2012). Early diagenetic dolomitization occurs in pore-water fluids whose chemistry reflects both the chemical composition of the original fluid (seawater, meltwater, or mixing of the two) as well as reactions that occur within the pore-fluid space (neomorphism, recrystallization, dolomitization, organic matter remineralization). According to this model, spatial and temporal variability in the geochemistry of the cap dolostone will reflect variations in the style of early diagenetic dolomitization (fluid- or sedimentbuffered, Higgins et al., 2018; Ahm et al., 2018).

Calcium ( $\delta^{44/40}$ Ca) and magnesium ( $\delta^{26}$ Mg) isotopes and major/minor element ratios (Mg/Ca and Sr/Ca) in carbonate sediments can be used to determine whether or not the Marinoan cap dolostone formed during early diagenetic alteration of aragonite or calcite. In contrast to primary dolomite precipitation, dolomites that form during early diagenesis are expected to record systematic covariation between  $\delta^{44/40}$ Ca values and  $\delta^{26}$ Mg values that reflect formation over a range of fluid- to sediment-buffered conditions

(Higgins et al., 2018; Ahm et al., 2018; Blättler et al., 2015; Fantle and Higgins, 2014). When combined with other geochemical proxies, such as  $\delta^{13}$ C values, it is possible to use Ca and Mg isotopes as a geochemical fingerprint to identify fluid- and sediment-buffered dolomitization, and thereby constrain the composition of the primary sediment and the dolomitizing fluid. Here we apply this approach to the basal Ediacaran cap dolostone with new measurements of  $\delta^{44/40}$ Ca values,  $\delta^{26}$ Mg values, and trace element ratios from 23 sections spanning four continents to determine the origin of the basal Ediacaran cap dolostone and how its chemistry reflects conditions in the aftermath of the Marinoan glaciation.

#### 2. Behavior of Ca and Mg isotopes during early diagenesis

Calcium in carbonate sediments and magnesium in dolomites are major components of the sedimentary mass and are inherently resistant to diagenetic alteration. However, carbonate  $\delta^{44/40}$ Ca and  $\delta^{26} \mathrm{Mg}$  values have been shown to be sensitive to diagenetic alteration under conditions where there is sufficient cation supply to overwhelm the calcium and magnesium in the sediment (by fluid advection or diffusion over short length-scales. Higgins et al., 2018; Fantle and Higgins, 2014; Fantle and DePaolo, 2007). For example, circulation of seawater through the Bahama Banks produces distinct covariation between  $\delta^{44/40}$ Ca and  $\delta^{26}$ Mg values in early diagenetic dolomites (Higgins et al., 2018; Ahm et al., 2018; Fantle and Higgins, 2014). Dolomite with low  $\delta^{44/40}$ Ca values and high  $\delta^{26}$ Mg values reflects formation under sediment-buffered conditions and retains many of the chemical signatures of the primary sediment. Dolomite with high  $\delta^{44/40}$ Ca values and low  $\delta^{26}$ Mg values reflects formation under fluid-buffered conditions and has a chemical composition that is set by the dolomitizing fluid (seawater, Fig. 1).

Based on these observations, we interpret variability of sedimentary  $\delta^{44/40}$ Ca values, that are associated with covariation in  $\delta^{26} Mg$  values in dolomites and Sr/Ca ratios in limestones, to be a product of change in mineralogy and early marine carbonate diagenesis (fluid- and sediment-buffered). We do not interpret these geochemical relationships in terms of changes in primary precipitation rates in the surface ocean or changes in global fluxes based on three reasons: First, early marine diagenesis is widespread in shallow-water carbonate sediments and a plausible mechanism for the formation of large volumes of sedimentary dolomite in the geological record (e.g., Vahrenkamp and Swart, 1994). Second, although laboratory experiments have shown covariation between Sr/Ca ratios and  $\delta^{44/40}$ Ca values as a function of different carbonate precipitation rates (Tang et al., 2008), it is unclear if these experiments translate to natural settings. Third, given that a similar relationship between Sr/Ca ratios and  $\delta^{44/40}$ Ca values exists for early marine diagenesis of primary aragonite - and that this relationship has been observed and quantified during early diagenesis in modern platform settings - our model strongly suggests that covariation between the two is not a unique indicator of rate-dependence in the water column (Ahm et al., 2018). As independent geochemical and petrographic evidence exist for primary aragonite in both the cap carbonate sequence and elsewhere in the geological record (Blättler and Higgins, 2017), we regard early diagenetic alteration of aragonite as a better null hypothesis for the observed covariation between Sr/Ca ratios and  $\delta^{44/40}$ Ca values in ancient marine carbonate sediments.

Although we do not interpret  $\delta^{44/40}$ Ca values as reflecting differences in primary precipitation rates in the surface ocean, the behavior of  $\delta^{44/40}$ Ca values in carbonate sediments during early marine diagenesis is a consequence of the rate dependence of Ca isotope fractionation in carbonate minerals (Higgins et al., 2018; Blättler et al., 2015; Fantle and Higgins, 2014). The slow precipitation rates associated with early marine diagenesis do

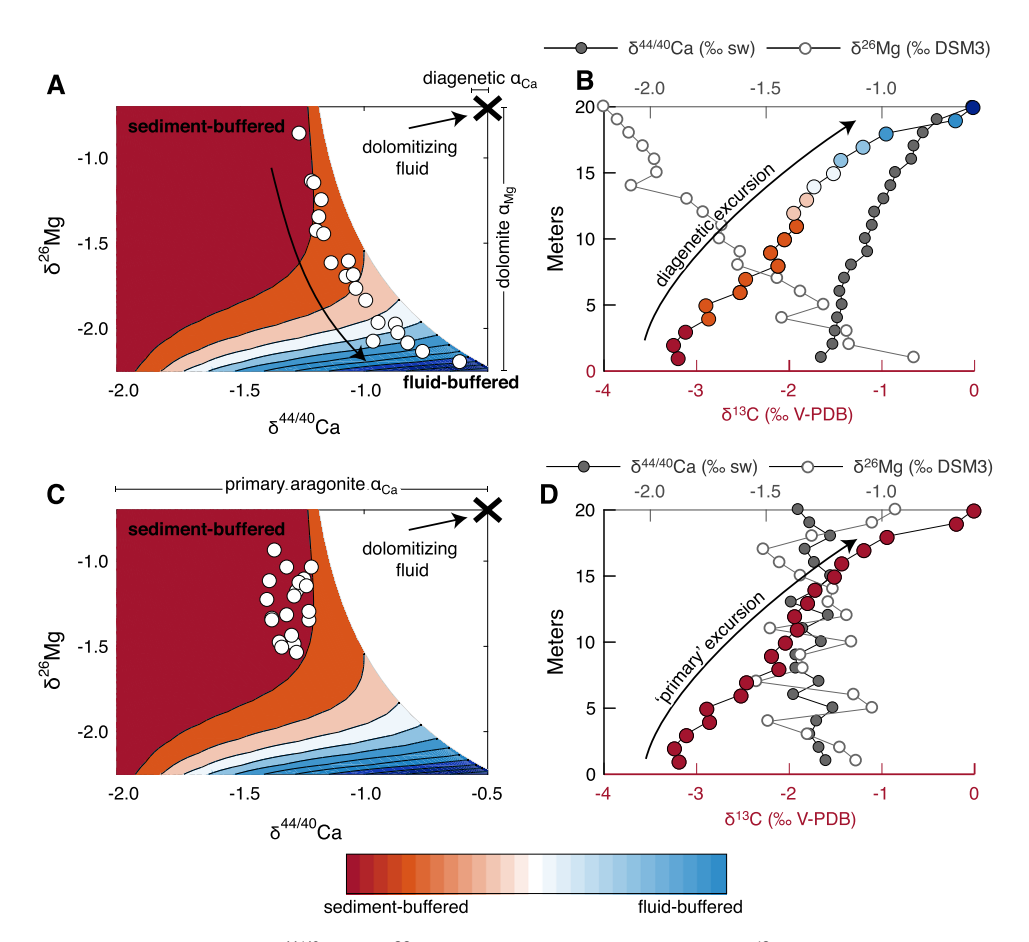


**Fig. 1.** Schematic figure showing the combined use of  $\delta^{44/40}$ Ca and  $\delta^{26}$ Mg values to distinguish if sedimentary  $\delta^{13}$ C values have been altered or preserved during early marine dolomitization. A synthetic dataset is used to illustrate the expected  $\delta^{44/40}$ Ca and  $\delta^{26}$ Mg isotope variability of samples that have been dolomitized during early marine fluid-buffered diagenesis (blue), and samples that have been dolomitized during sediment-buffered diagenesis (red). (A) Covariation between  $\delta^{44/40}$ Ca and  $\delta^{26}$ Mg values, and their relationship to the  $\delta^{13}$ C values, indicate that the stratigraphic trend in (B) is a product of changes in the diagenetic regime, from sediment-buffered dolomitization ( $\sim$ 0–5 m) towards increasingly more fluid-buffered dolomitizing. (C) In contrast, low  $\delta^{44/40}$ Ca values and high  $\delta^{26}$ Mg values indicate sediment-buffered dolomitization where the primary  $\delta^{13}$ C values and stratigraphic trend (D) have been preserved. Using the modeled covariation between  $\delta^{44/40}$ Ca and  $\delta^{26}$ Mg values, it is possible to distinguish stratigraphic trends that are primary from those that reflect changes in the diagenetic regime. Note that the specific shape of the Ca and Mg isotope phase-space is a function of the geochemistry of the primary mineral, the secondary mineral, and the diagenetic fluid (e.g., there would be a different phase-space for aragonite neomorphism or meteoric diagenesis). (For interpretation of the colors in the figure(s), the reader is referred to the web version of this article.)

not appreciably fractionate Ca isotopes (Fantle and DePaolo, 2007; Jacobson and Holmden, 2008). In contrast, the precipitation rates associated with biotic and abiotic precipitation of primary carbonate minerals in the surface ocean are orders of magnitude higher and can lead to significant fractionation of Ca isotope;  $\sim -1.6\%$  for aragonite and  $\sim -1.1\%$  for calcite (Gussone et al., 2005). Critically, the range in  $\delta^{44/40}$ Ca values that results from variations in carbonate mineralogy and rate-dependent Ca isotope fractionation during diagenesis are significantly larger than plausible changes in seawater  $\delta^{44/40}$ Ca values associated with transient perturbations to the global calcium cycle (Komar and Zeebe, 2016; Husson et al., 2015; Blättler and Higgins, 2017). Therefore, in contrast to previous studies we do not interpret Ca isotope variation in the cap carbonate sequence to reflect changes in global weathering rates (cf. Kasemann et al., 2005, 2014; Silva-Tamayo et al., 2010).

The behavior of Mg isotopes during early diagenetic dolomitization is characterized by Rayleigh-type distillation of the pore-fluid due to the large fractionation factor associated with dolomite precipitation in a wide range of diagenetic environments ( $\sim -2\%$ , Higgins and Schrag, 2010). As magnesium is removed from the pore-fluid, the  $\delta^{26}$ Mg values of the residual fluid increases, producing dolomites with yet higher  $\delta^{26}$ Mg values farther along the path of fluid transport (Fig. 1). In contrast, fluid-buffered dolomites formed in pore-waters close to the origin of fluid flow will have relatively lower  $\delta^{26}$ Mg values.

The systematic covariation between  $\delta^{26} \rm Mg$  and  $\delta^{44/40} \rm Ca$  values in early diagenetic dolomites also provides additional insights into the origins and preservation of  $\delta^{13} \rm C$  values in carbonates rocks. As the ratio of calcium and carbon are similarly abundant in seawater and carbonates, their behavior during fluid-buffered and sediment-buffered early marine diagenesis is expected to be similar (Ahm et al., 2018). Samples where  $\delta^{13} \rm C$  values have been reset during dolomitization are expected to have high  $\delta^{44/40} \rm Ca$  and low  $\delta^{26} \rm Mg$  values whereas samples where the primary  $\delta^{13} \rm C$  values of the carbonate sediment (e.g., aragonite) are preserved are expected to have low  $\delta^{44/40} \rm Ca$  values and high  $\delta^{26} \rm Mg$  values (Fig. 1).

#### 3. Background and methods

#### 3.1. Sample suite

Our sample suite consists of 23 stratigraphic sections from southern Africa, North America, South Australia, and Mongolia. The geological context for each section comes from previously published work that includes  $\delta^{13}$ C and  $\delta^{18}$ O values (Bold et al., 2016; Hoffman et al., 2007; Hoffman and Macdonald, 2010; Hoffman, 2011; Macdonald et al., 2009, 2013a, 2013b; Rose and Maloof, 2010) and is supplemented by new measurements from sections from northwest Canada (Strauss, unpublished). A brief summary of the settings for individual sections is outlined in Appendix A.

#### 3.2. Methods

Ca isotope measurements from the cap carbonate sequence are reported as the relative abundance of  $^{44}\text{Ca}$  relative to  $^{40}\text{Ca}$  using standard delta notation, normalized to the isotopic composition of modern seawater. For Ca isotopes, the external reproducibility for SRM915b and SRM915a relative to modern seawater is  $-1.19\pm0.14\%$  ( $2\sigma$ , N=120) and  $-1.86\pm0.16\%$  ( $2\sigma$ , N=24), respectively. Similarly, Mg isotope ratios are expressed as the relative abundance of  $^{26}\text{Mg}$  versus  $^{24}\text{Mg}$ , normalized to DSM3. For Mg, the long-term external reproducibility for Cambridge-1 and seawater are  $-2.61\pm0.10\%$  ( $2\sigma$ , N=81) and  $-0.83\pm0.10\%$  ( $2\sigma$ , N=47), respectively. We refer to Appendix B and previous publications for a detailed outline of the Ca and Mg isotope analyses and major and trace element analyses performed at Princeton University (Higgins et al., 2018; Blättler et al., 2015; Husson et al., 2015).

#### 3.3. Description of diagenetic model

To constrain the origin of geochemical signatures in the cap carbonates, we model carbonate diagenesis/dolomitization using a numerical model (Ahm et al., 2018). The model simulates early marine carbonate diagenesis through the dissolution of primary calcium carbonate and re-precipitation of dolomite or low-Mg calcite along a flow path (please refer to Ahm et al. (2018) for full details on the model setup). The term neomorphism is used to describe the conversion of aragonite to low-Mg calcite, while the term dolomitization is used to describe the conversion of calcium carbonate to dolomite. Observations from modern carbonate platforms indicate that fluid flow is dominated by advection (Henderson et al., 1999; Higgins et al., 2018). We assume that the basal Ediacaran cap dolostones were dolomitized within 10<sup>5</sup> kyr. This assumption implies that fluid flow and dolomitization rates were approximately an order of magnitude higher than rates estimated from modern platform environments (~0.1% kyr<sup>-1</sup> and  $\sim$ 10 cm yr<sup>-1</sup>, Higgins et al., 2018; Ahm et al., 2018; Henderson et al., 1999). As a result, we set reaction rates to 1% kyr<sup>-1</sup> and flow rates to 1.2 myr<sup>-1</sup>, but since we evaluate our model output in cross-plots space, our model results are not sensitive to changes in either reaction rates or flow rates (Ahm et al., 2018). The model output is a ternary phase-space between pairs of geochemical proxies that is defined by the geochemistry of the primary sediment, the fluid-buffered, and the sediment-buffered end-members. By identifying the fluid- and sediment-buffered end-members, we can use the model to predict the composition of the primary sediment and the diagenetic fluid.

The model is fit to the distribution of geochemical data by estimating the composition of the diagenetic fluid and primary sediment. Model results are optimized by minimizing the orthogonal difference between samples and the model phase-space (the residual). In addition, to ensure consistent predictions across different proxies, the position and shape of the model phase space is constrained by the percentage of alteration. For example, samples that are modeled as 100% dolomitized in the phase-space of  $\delta^{44/40}$ Ca versus  $\delta^{26}$ Mg values, should also be 100% dolomitized in the phase-space of  $\delta^{44/40} \text{Ca}$  versus  $\delta^{13} \text{C}$  values. Samples that are less than 100% recrystallized in this model phases space are interpreted to be only partially altered during early marine diagenesis (Ahm et al., 2018). These samples are subsequently stabilized during later burial diagenesis in conditions that are sedimentbuffered, thus preserving the geochemical signals associated with early marine diagenesis. In other words, our model does not assume that samples do not undergo subsequent diagenetic recrystallization (neomorphism) during burial, simply that this recrystallization must have been sediment-buffered to preserve the geochemical signature of early marine diagenesis. We refer to Appendix C for sensitivity tests and optimization of model results (Figs. C.11–C.12).

#### 4. Results

#### 4.1. Congo craton (Namibia)

The Keilberg cap dolostone (Hoffman et al., 2007; Hoffman, 2011) exhibits little stratigraphic variability in  $\delta^{44/40}\mathrm{Ca}$  and  $\delta^{26}\mathrm{Mg}$  values within individual sections, but there are systematic trends across the Otavi platform in northern Namibia (Fig. 2). The platform interior (sections P4017 and P7500) is characterized by relatively low  $\delta^{44/40}\mathrm{Ca}$  values between  $\sim -1$  and -1.3% and high  $\delta^{26}\mathrm{Mg}$  values between  $\sim -1.5$  and -1.0%. On the outer platform (P7016),  $\delta^{44/40}\mathrm{Ca}$  are consistently higher  $\sim -0.7\%$  and  $\delta^{26}\mathrm{Mg}$  values are consistently lower  $\sim -1.9\%$ , in agreement with findings from previous studies (Kasemann et al., 2005, 2014). In contrast, a section (P7017) on the distal foreslope of the platform has  $\delta^{44/40}\mathrm{Ca}$  values  $\sim -1\%$  and  $\delta^{26}\mathrm{Mg}$  values  $\sim -1.7\%$ , a range similar to sections from the platform interior. Across all cap dolostone sections, there is clear positive covariation between  $\delta^{13}\mathrm{C}$  and  $\delta^{44/40}\mathrm{Ca}$  values and a negative covariation between  $\delta^{13}\mathrm{C}$  and  $\delta^{26}\mathrm{Mg}$  values.

The overlying transgressive limestone unit of the Maieberg Formation (Fm.) is characterized by lower  $\delta^{26}{\rm Mg}$  and  $\delta^{44/40}{\rm Ca}$  values than the dolostone (upper part of section P4017). A  $\sim$ 1% decline in  $\delta^{26}{\rm Mg}$  values down to  $\sim$  -2% is mirrored by stratigraphic variability in  $\delta^{44/40}{\rm Ca}$  values.  $\delta^{44/40}{\rm Ca}$  values increase to -0.8% followed by a decrease down to -1.4%. The most negative  $\delta^{44/40}{\rm Ca}$  values in the Maieberg limestone correlate with higher Sr/Ca ratios (Fig. 2). In contrast to the underlying dolostone, in the Maieberg limestone samples with lower  $\delta^{13}{\rm C}$  values correlate with higher  $\delta^{44/40}{\rm Ca}$  values and lower  $\delta^{26}{\rm Mg}$  values. In addition, lower  $\delta^{44/40}{\rm Ca}$  values in the limestone covary with higher Sr/Ca ratios.

#### 4.2. Kalahari craton (Namibia)

The Dreigratberg cap dolostone in southwest Namibia (section F817) consists of limestone overlain by dolostone (Hoffman and Macdonald, 2010). The limestone hosts rare ice-rafted debris that marks the retreat of the ice-line and records a fall in relative sealevel prior to the surface of maximum flooding at the top of the overlying dolostone (Hoffman and Macdonald, 2010). There is no isotopic offset in  $\delta^{44/40}$ Ca values between the limestone and dolostone but there is a steady stratigraphic increase from -1.5 toward -1% towards the top of the section. In contrast,  $\delta^{26}$ Mg values in the lower limestone unit record a negative excursion from -1.5 to -2.5%. The limestone unit also has higher Sr/Ca ratios than the overlying dolostone (Fig. 2).

#### 4.3. South Australia

The Nuccaleena cap dolostone in the Flinders Ranges, South Australia, was deposited across a large central anticline and a series of half-grabens to the north, which together span platform to basinal settings (Rose and Maloof, 2010). The Nuccaleena cap dolostone units have a large range in  $\delta^{13}\mathrm{C}$  values (between -8 and +2%, Rose and Maloof, 2010), but a relatively small range in  $\delta^{44/40}\mathrm{Ca}$  values (between  $\sim-1.2$  and -0.7%). Platform dolostone sections in the South and Central Flinders (N250, N255) and upper slope facies south of the Mt Fitton anticline (N288) have relatively invariant  $\delta^{44/40}\mathrm{Ca}$  values ( $\sim-1\%$ ) and  $\delta^{26}\mathrm{Mg}$  values ( $\sim-2\%$ ) and there is broad covariation between higher Sr/Ca ratios and lower  $\delta^{44/40}\mathrm{Ca}$  values (Fig. 3).

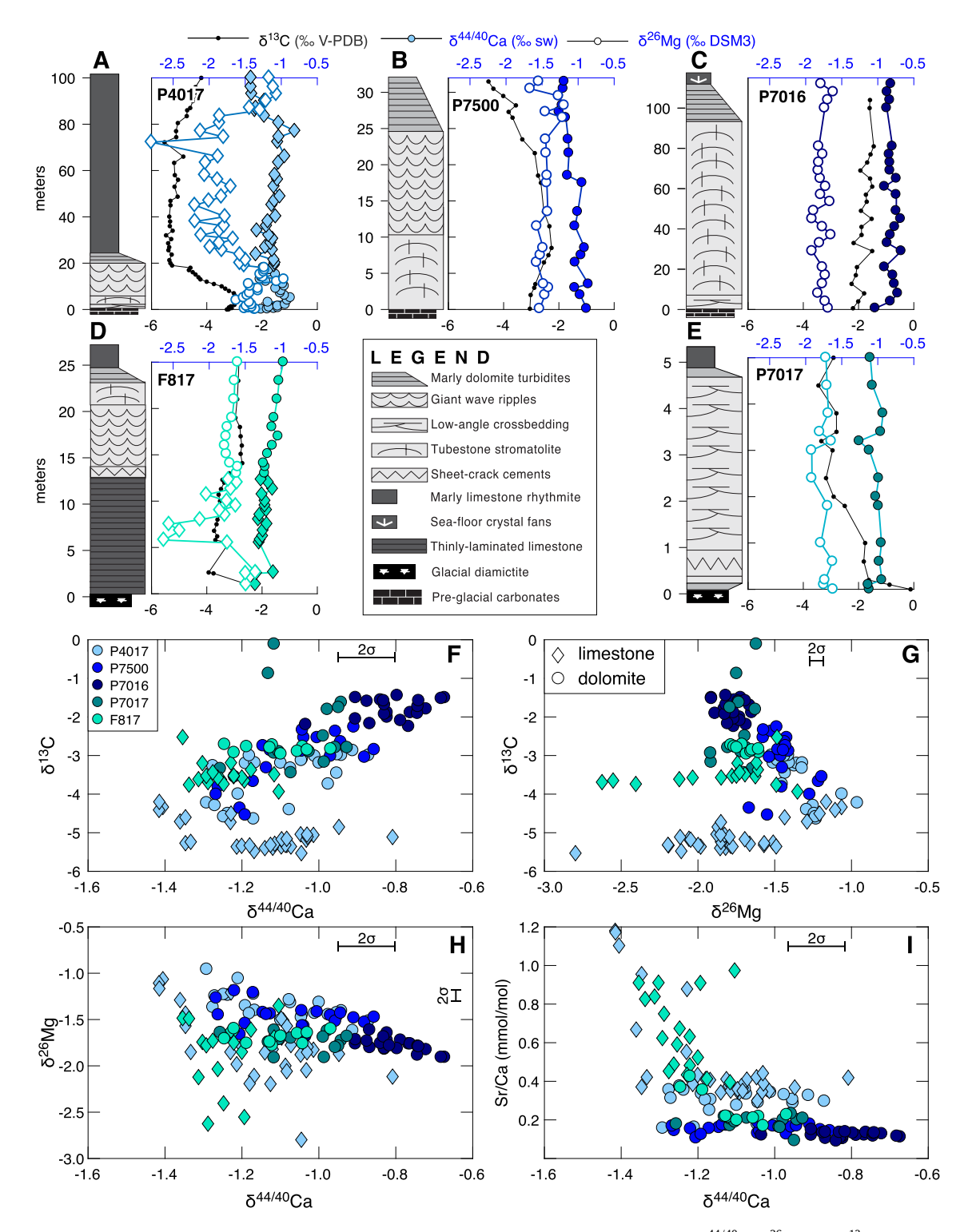


**Fig. 2. Chemostratigraphy from the Dreigratberg and Keilberg cap carbonate, Namibia.** (A–E) Lithostratigraphy with  $\delta^{44/40}$ Ca,  $\delta^{26}$ Mg, and  $\delta^{13}$ C values from Congo craton, Namibia (P4017, P7500, P7016, P7017, Hoffman et al., 2011) and Kalahari craton, Namibia (F817, Hoffman and Macdonald, 2010). The deep water Maieberg limestones that are deposited on the Keilberg cap carbonate are included in section P4017. Sections are broadly aligned from shallow platform settings on the left towards platform margin and deeper foreslope settings on the right. (F–I) Crossplots comparing data from all five sections. Notice that circles represent dolomite and diamonds represent limestone.

In contrast, the geochemistry of dolostone sections north of the Mt Fitton anticline are more variable with  $\delta^{44/40}$ Ca values between  $\sim -1.2$  and -0.7% and  $\delta^{26}$ Mg values  $\sim -3$  and -1.6% (Fig. 3). Limestones deposited in upper slope facies in the shallowest part of the Mt Fitton anticline (C213) are both more enriched in  $^{44}$ Ca ( $\sim -0.58\%$ ) and more depleted in  $^{26}$ Mg ( $\sim -4.4\%$ ) relative to the basinal dolostones (C212, C215). In addition, these limestones

have low  $\delta^{13}$ C values correlating with high  $\delta^{44/40}$ Ca values and low  $\delta^{26}$ Mg values, whereas the dolostones have low  $\delta^{13}$ C values correlating with low  $\delta^{44/40}$ Ca values and high  $\delta^{26}$ Mg values.

#### 4.4. Laurentia (Death Valley)

The Noonday cap carbonate (the Sentinel Peak Member) is dolomitized on the platform but is preserved as limestone in

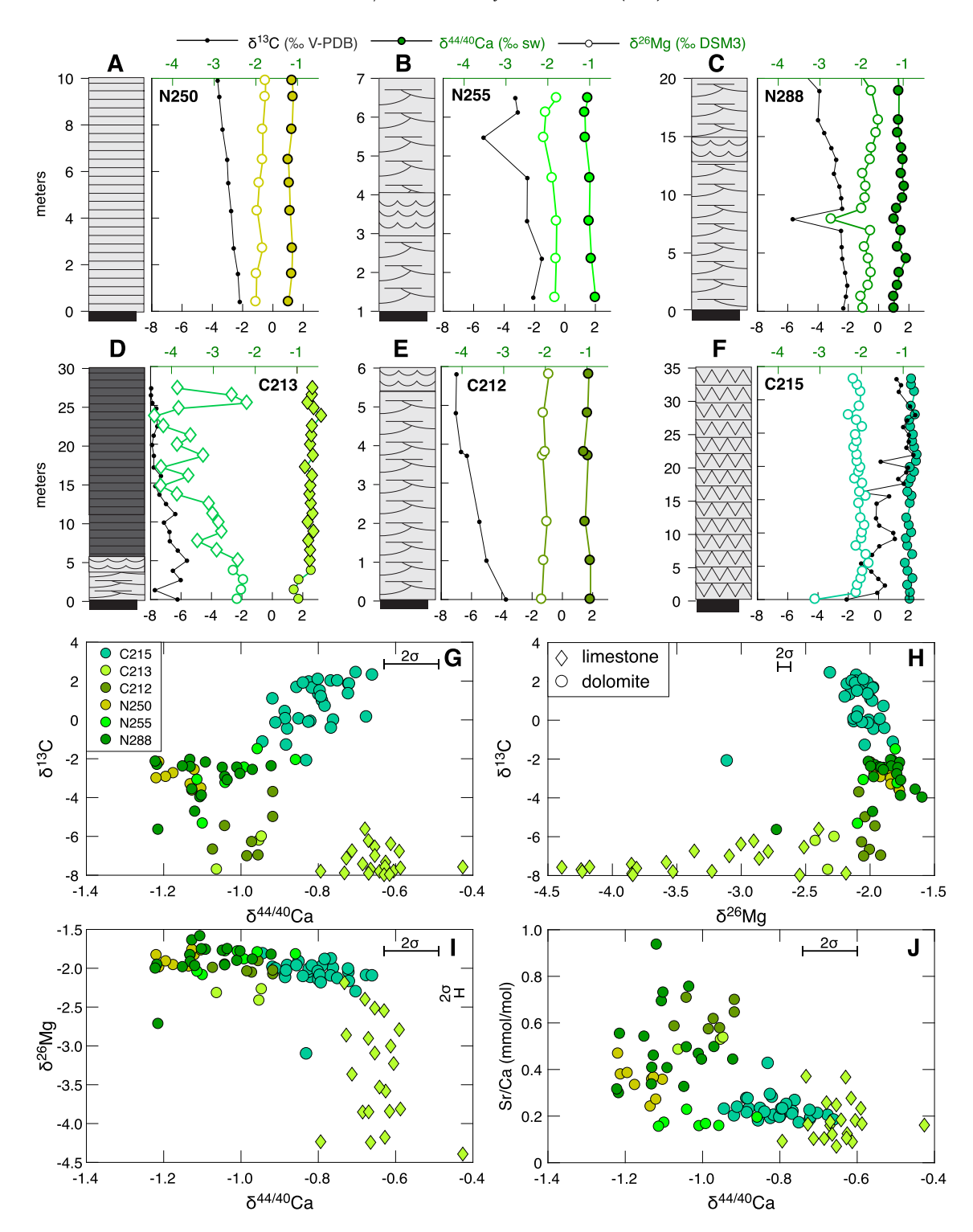


Fig. 3. Chemostratigraphy from the Nuccaleena cap carbonate, South Australia. (A–F) Lithostratigraphy with  $\delta^{44/40}$ Ca,  $\delta^{26}$ Mg, and  $\delta^{13}$ C values from south Australia (N250, N255, N288, C212, C213, C215, Rose and Maloof, 2010). For legend see Fig. 2. Sections are broadly aligned from shallow platform settings on the left towards platform margin and deeper foreslope settings on the right. (G–J) Crossplots comparing data from the six sections. Notice that circles represent dolomite and diamonds represent limestone.

deeper foreslope settings (Silurian Hills, Macdonald et al., 2013a). In general, the platform dolostone (F1344) has higher  $\delta^{44/40}$ Ca values and lower  $\delta^{26}$ Mg values than the deeper water limestones (F1340) and associated dolostone olistoliths (F1341). In contrast to the low  $\delta^{26}$ Mg values and high  $\delta^{44/40}$ Ca values in the Nuccaleena limestones, the deepwater Noonday limestones have the highest  $\delta^{26}$ Mg values (up to  $\sim -0.6\%$ ) and the lowest  $\delta^{44/40}$ Ca values (down to  $\sim -1.9\%$ ). In addition, the low

 $\delta^{44/40}$ Ca values in the limestone correlate with high Sr/Ca ratios (Fig. 4).

#### 4.5. Laurentia (Arctic Alaska)

The Nularvik cap dolostone (F601) has  $\delta^{13}$ C values between 0 and -2% (Macdonald et al., 2009). The  $\delta^{13}$ C values are inversely correlated with  $\delta^{44/40}$ Ca values between -1.3 and -0.8%.

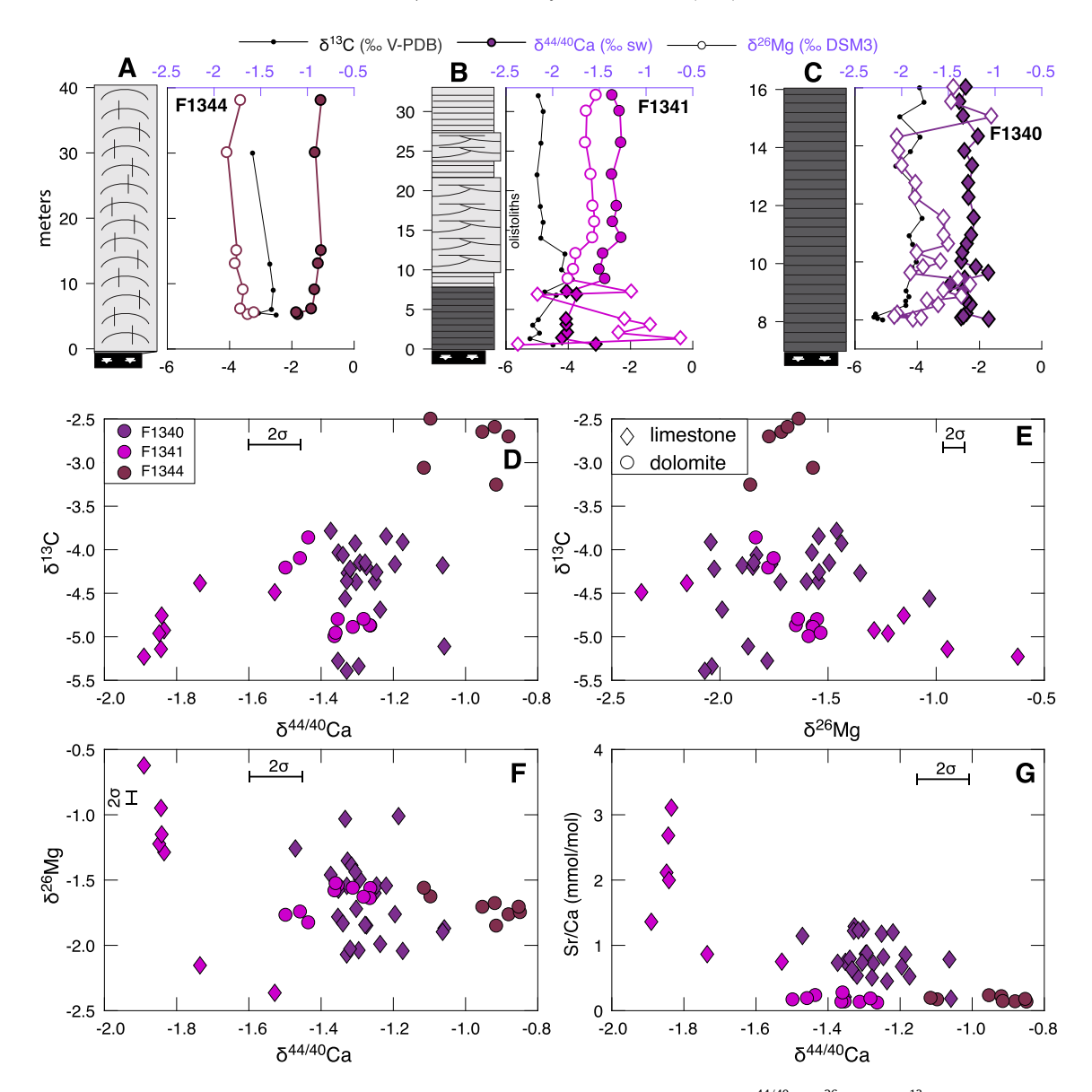


**Fig. 4.** Chemostratigraphy from the Noonday cap carbonate, Death Valley, California. (A–C) Lithostratigraphy with  $\delta^{44/40}$ Ca,  $\delta^{26}$ Mg, and  $\delta^{13}$ C values from Death Valley (F1344, F1341, F1340, Macdonald et al., 2013a). For legend see Fig. 2. Sections are broadly aligned from shallow platform settings on the left towards platform margin and deeper foreslope settings on the right. (D–G) Crossplots comparing data from the three sections. Notice that circles represent dolomite and diamonds represent limestone.

(Fig. 5E), while  $\delta^{26}$ Mg values are relatively invariable between -2 and -1.7%.

#### 4.6. Laurentia (Northwest Canada)

The  $\delta^{13}$ C values in the Ravensthroat cap dolostone in the Mackenzie Mountains (J1132, P7D, Macdonald et al., 2013b), Ogilvie Mountains (J1713), and Tatonduk region (J1402, Strauss, unpublished) span a range from  $\sim$  –7 to 0%. The values in the overlying Hayhook limestone unit are less variable ( $\sim$  –5%). In contrast to the  $\delta^{13}$ C values,  $\delta^{44/40}$ Ca values are more variable in the limestone unit (between –2 and –0.6%) than in the underlying dolostone (between  $\sim$  –1.2 and –0.6). Similarly, the  $\delta^{26}$ Mg values in the limestone span a larger range (between –3 and –1%) than in the dolostone (between –2 and –1.3%). As a result, there is a more pronounced covariation between  $\delta^{13}$ C,  $\delta^{26}$ Mg, and  $\delta^{44/40}$ Ca values in the dolostone compared to the limestone (Fig. 5).

Hayhook Aragonite fans In the Mackenzie Mountains, the lowest  $\delta^{44/40}$ Ca values ( $\sim -2\%$ ) are found in calcite pseudomorphs after aragonite fans in the limestones of the Hayhook Fm. (AF; Fig. 5).  $\delta^{44/40}$ Ca values down to -2% and elevated Sr/Ca ratios rarely are found in carbonate rocks between  $\sim 3$  and 0.5 Ga (Blättler and Higgins, 2017), matched only during the recovery of the Ediacaran Shuram-Wonoka CIE (Husson et al., 2015). Targeted sampling of the fans and the infilling matrix reveal a consistent offset in the geochemical signature of these two texturally distinct phases. The gray fans have lower  $\delta^{44/40}$ Ca values, higher  $\delta^{13}$ C, and lower  $\delta^{26}$ Mg values than the pink mud matrix (Fig. A.10). The trace element ratios also are offset between fans and matrix, with higher Sr/Ca ratios and lower Mg/Ca ratios in the fans compared to the matrix.

#### 4.7. Mongolia

In Mongolia,  $\delta^{13}$ C values of the Ol cap dolostone span  $\sim$ 10% across the Zavhkhan Terrane (Fig. 6, Bold et al., 2016). The highest values are found in sections from the inner platform (F875, U1113)

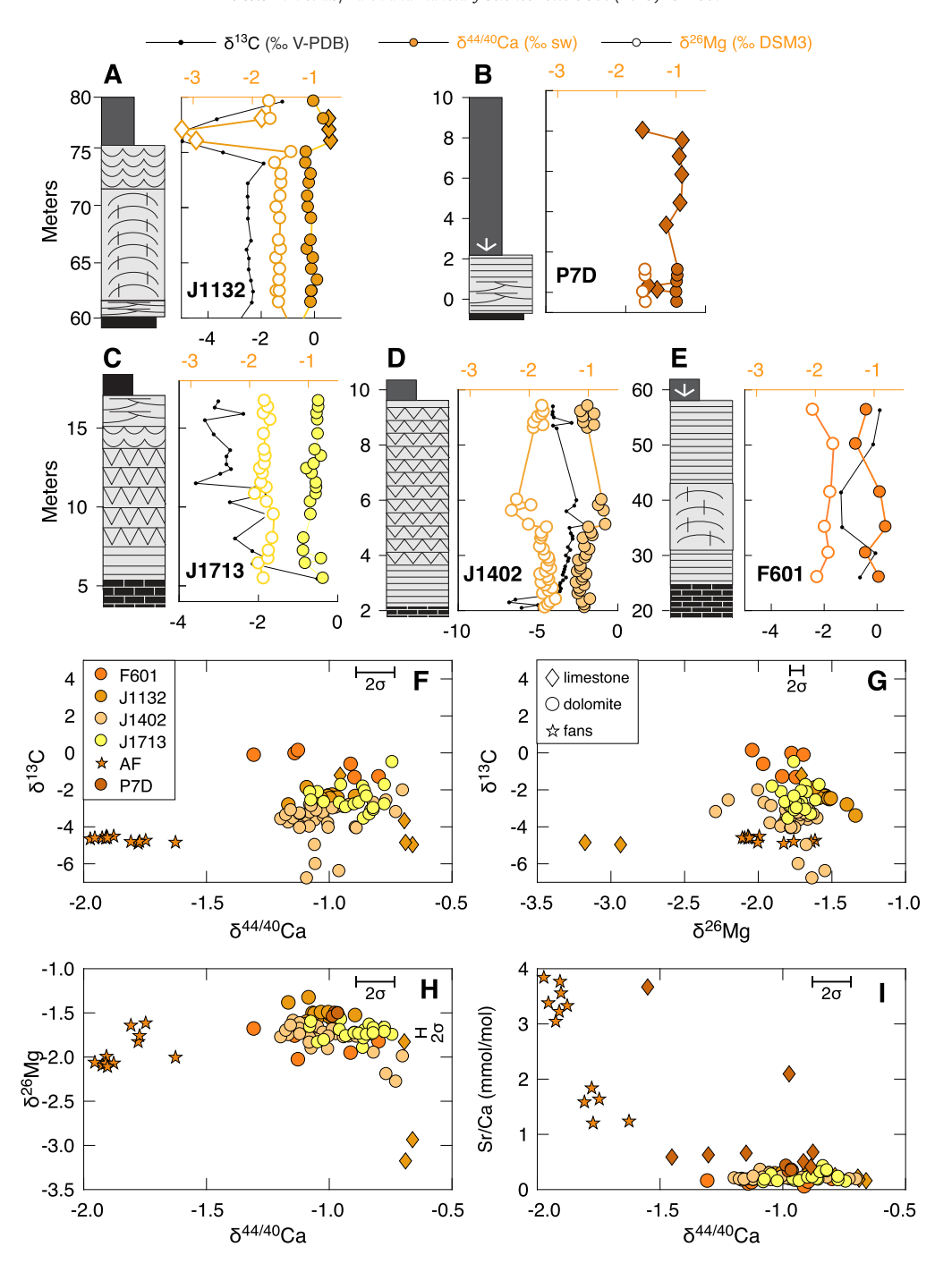


**Fig. 5. Chemostratigraphy from the Ravensthroat cap carbonate, Northwest Canada and Alaska.** (A–B) Lithostratigraphy with  $\delta^{44/40}$ Ca,  $\delta^{26}$ Mg, and  $\delta^{13}$ C values from Northwest Canada, where the Ravensthroat cap dolomites are overlain by limestones from the Hayhook Formation (J1713, J1132, P7D, J1402, Macdonald et al., 2013b), and (C–D) from Arctic Alaska (F601 Macdonald et al., 2009). For legend see Fig. 2. (E–H) Cross-plots comparing data from the four sections. Notice that circles represent dolomite, diamonds represent limestone, and stars represent aragonite fans.

that are more pervasively dolomitized than the basinal sections (Bold et al., 2016). In general, these platform sections have higher  $\delta^{44/40}\mathrm{Ca}$  values (up to -0.8%) and lower  $\delta^{26}\mathrm{Mg}$  values (down to -2%). In contrast, in the basinal sections (F708, F860),  $\delta^{44/40}\mathrm{Ca}$  values are variable between -1 and -1.5%, whereas  $\delta^{26}\mathrm{Mg}$  values are relatively invariant between -1.5 and -1.7%. Combined,  $\delta^{13}\mathrm{C}$  values covary with  $\delta^{26}\mathrm{Mg}$  values across all sections with a less clear relationship between  $\delta^{13}\mathrm{C}$  and  $\delta^{44/40}\mathrm{Ca}$  values. In addition,  $\delta^{44/40}\mathrm{Ca}$  values do not seem to show any distinctive correlation to Sr/Ca ratio, in contrast to trends from other localities.

The geochemical signature of cap dolostone samples from Mongolia are consistently offset from sections in Australia, Namibia, and North America. Specifically, the  $\delta^{13}$ C values of the Mongolian samples are higher than in other sections (up to +8‰, Fig. 6). The range in values observed in Mongolia has been linked to a regionally expansive dolomitization front that penetrates the basal Ediacaran dolostone and underlying glacial and pre-glacial sediments (Bold et al., 2016). We therefore attribute the enriched  $\delta^{13}$ C values in the Mongolia cap dolostone to the local history of dolomitization and fluid flow (Bold et al., 2016). Discussion of the origin of the Ol cap carbonate is limited to the supplementary material and is not discussed further below.

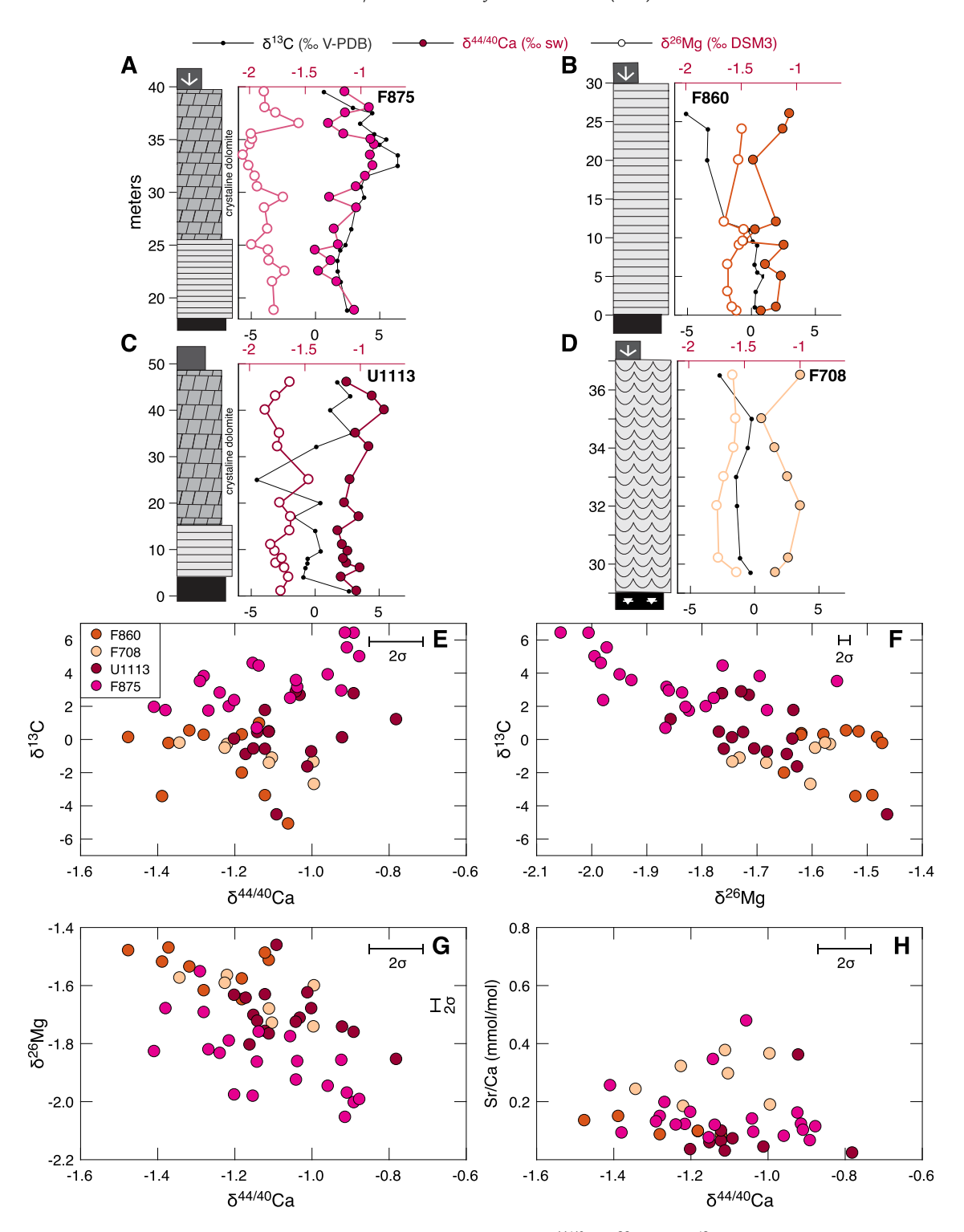


**Fig. 6. Chemostratigraphy from the OI cap carbonate, Mongolia.** (A–D) Lithostratigraphy with  $\delta^{44/40}$ Ca,  $\delta^{26}$ Mg, and  $\delta^{13}$ C values from Mongolia (F875, U1113, F708, F860, Bold et al., 2016). For legend see Fig. 2. Sections are broadly aligned from shallow platform settings on the left towards platform margin and deeper foreslope settings on the right. (E–H) Crossplots comparing data from the four sections.

#### 5. Discussion

Despite the geochemical heterogeneity between and within individual margins,  $\delta^{44/40} \text{Ca}$  and  $\delta^{26} \text{Mg}$  values in the cap dolostone covary across all localities – dolostones with low  $\delta^{44/40} \text{Ca}$  values have high  $\delta^{26} \text{Mg}$  values and dolostones with high  $\delta^{44/40} \text{Ca}$  values have low  $\delta^{26} \text{Mg}$  values (Figs. 8–9). This covariation is similar to observations from Neogene dolomites (Higgins et al., 2018; Blättler et al., 2015) and is consistent with formation of early di-

agenetic dolomite formed under a range of diagenetic conditions (fluid- to sediment-buffered, see section 2). The appearance of similar covariation in cap dolostone units from across the globe provides evidence that cap dolostones formed by the early diagenetic conversion of a precursor carbonate mineral and not by primary precipitation from the surface ocean (Fig. 1). In subsequent sections, we explore the implications of this result using the bulk geochemistry of carbonate sediments ( $\delta^{44/40}$ Ca,  $\delta^{26}$ Mg,  $\delta^{13}$ C values, and Sr/Ca ratios) together with a numerical model of

early marine diagenesis to characterize the chemistry and isotopic composition of the primary carbonate minerals and the diagenetic fluids. These model results then are used to reconstruct the environmental conditions associated with cap carbonate deposition and dolomitization in the aftermath of the Marinoan glaciation.

#### 5.1. Primary cap carbonate mineralogy

Three lines of evidence indicate that aragonite was the precursor carbonate mineral for the entire cap carbonate sequence. First, many dolostone units are characterized by  $\delta^{44/40}$ Ca values that are significantly lower ( $\sim < -1\%$ ) than expected for dolomitized calcite or primary dolomite ( $\sim > -1\%$ , Gussone and Dietzel, 2016; Higgins et al., 2018; Ahm et al., 2018). Second, petrographic observations and sub-sampling of relict aragonite fans (now calcite) from the Hayhook Fm. in Northwest Canada are characterized by low  $\delta^{44/40}$ Ca values (-2%) and high Sr/Ca ratios (3-4 mmol/mol, Fig. A.10). Although the micritic matrix has slightly higher  $\delta^{44/40}$ Ca values (-1.6%) and lower Sr/Ca ratios (1-2 mmol/mol), the values are still within the range of those expected for neomorphosed aragonite (e.g., Ahm et al., 2018). Relict aragonite fans also are preserved as dolomite in Arctic Alaska and Mongolia (Macdonald et al., 2009; Bold et al., 2016). Third, both limestone and dolomite cap carbonates with elevated Sr/Ca ratios tend to have low  $\delta^{44/40}$ Ca values (Figs. 8-9), a relationship that is similar to that observed for diagenesis of primary aragonite in the Bahamas (Higgins et al., 2018), and indistinguishable from the co-variation between  $\delta^{44/40}\text{Ca}$  values and Sr/Ca ratios observed in the aragonite fans and micrite of the Hayhook Fm. (Fig. 5).

#### 5.2. Predictions for diagenesis and fluid flow in the glacial aftermath

Field observations can constrain the timing and relationship between aragonite precipitation, early dolomitization, and Snowball Earth deglaciation. First, the cap dolostone contains wavegenerated sedimentary structures indicating that deposition occurred above storm wave-base during the initial kiloyears of sealevel rise (Hoffman et al., 2011; Rose and Maloof, 2010; Macdonald et al., 2013a, 2013b; Hoffman and Macdonald, 2010; Bold et al., 2016). As a result, the chemical composition of the primary sediment likely reflected precipitation from the growing meltwater surface ocean (Shields, 2005; Liu et al., 2014; Yang et al., 2017). Second, the widespread occurrence of temporally coincident early diagenetic cap dolostone units (with consistent covariance between Ca and Mg isotopes) indicate that the primary sediment was dolomitized shortly after deposition during the initial stages of deglaciation. Third, the stratigraphic transition from dolostone to deeper-water limestone suggests a decrease in dolomitization near the time of maximum flooding.

#### *5.2.1. The chemistry of the meltwater lens*

The stratigraphic constraints outlined above suggest that the chemistry of the precursor aragonite reflects the chemistry of the meltwater surface ocean. Previous studies have suggested that the meltwater surface ocean was dominated by inputs from the rapid weathering of carbonates in the high  $p\text{CO}_2$  glacial aftermath (Hoffman and Schrag, 2002; Higgins and Schrag, 2003). Chemical weathering of carbonate-dominated terrains produce waters with low  $\delta^{44/40}\text{Ca}$  and  $\delta^{26}\text{Mg}$  values due to the low values of continental carbonates ( $\delta^{44/40}\text{Ca} = -1\%$ ,  $\delta^{26}\text{Mg} = -2\%$ ). For example, freshwater discharge through carbonate sediments in Florida Bay produce Ca-rich groundwater (Ca<sup>2+</sup>  $\sim$  13.5 mmol/kg) with low  $\delta^{44/40}\text{Ca}$  values between -0.4 and -0.9%. As a result, bulk carbonate sediments in the bay are characterized by  $\delta^{44/40}\text{Ca}$  values down to  $\sim -2\%$  (Holmden et al., 2012). In contrast, the concentrations of Mg in groundwater aquifers are orders of magnitudes

lower than in seawater (e.g.,  $\sim$ 0.6–2 mmol/kg in the Madison aquifer; Jacobson et al., 2010). Mg isotopes in carbonate-dominated groundwater systems are low ( $\sim$  –1.6 and –1.0‰) with travertine deposits recording  $\delta^{26}$ Mg values down to –4‰ (Tipper et al., 2006; Jacobson et al., 2010). Relict aragonite fans in limestones from the cap carbonate sequence have both  $\delta^{44/40}$ Ca values and  $\delta^{26}$ Mg values that approach  $\sim$  –2‰, consistent with formation in a meltwater surface ocean. Accounting for the fractionation between aragonite and fluid (Gussone et al., 2005; Wang et al., 2013), these measured values predict a meltwater lens with  $\delta^{44/40}$ Ca values of  $\sim$  –0.4‰ and  $\delta^{26}$ Mg values of  $\sim$  –1‰, similar to the range of observations in the modern settings outlined above (Table 1).

#### 5.2.2. The chemistry of glacial seawater

Widespread dolomitization of aragonite precipitated from a meltwater surface ocean requires a large supply of Mg. Considering the low Mg concentrations of freshwater (see above), we hypothesize that the dolomitizing fluid was glacial seawater. Previous studies have suggested that the chemical composition of glacial seawater was controlled by hydrothermal alteration of oceanic crust due to a reduction in continental inputs during the global glaciation (Hoffman and Schrag, 2002). As Mg is removed from seawater in both low and high-temperature hydrothermal systems, prolonged global glaciation will tend to lower seawater Mg concentrations relative to ice-free conditions. This mechanism is similar to models for the near continent free Archean (Jones et al., 2015). As a result, Mg/Ca ratios in glacial seawater are expected to be lower in comparison with Cenozoic seawater ratios, although still substantially higher than ratios expected for freshwaters (see above), and lower than the general conditions thought to characterize the Proterozoic (Jones et al., 2015). Similarly, a reduction in carbonate burial, increase in seafloor dissolution (Hoffman and Schrag, 2002), and continued high-temperature hydrothermal alteration are expected to have raised Ca concentrations and lowered  $\delta^{44/40}$ Ca values relative to pre-glacial seawater. Given these assumptions, we expect that glacial seawater was characterized by relatively low Mg/Ca ratios, low  $\delta^{44/40}$ Ca values, and high  $\delta^{26}$ Mg values (Table 1).

### 5.2.3. Fluid circulation in platform sediments during the glacial aftermath

Deglaciation and meltwater discharge in coastal zones provides a physical mechanism to circulate seawater through carbonate platforms worldwide (Fig. 7). During the development of an expansive meltwater wedge in coastal areas, density gradients between meltwater and glacial seawater promote buoyant convection of fluids within platform sediments (Wilson, 2005; Cooper et al., 1964; Reilly and Goodman, 1985). The less dense meltwater forms a wedge and flows seawards to displace more dense seawater (Fig. 7A). In the transition zone between meltwater and seawater, seawater is diluted and entrained in the upward flow of freshwater through turbulent mixing (Cooper et al., 1964). To compensate the seaward flow of diluted waters, seawater flows landward from the

**Table 1**Summary of expectations and model results (see Appendix C for sensitivity tests of model optimization results).

Variable	Meltwater	Seawater	Primary aragonite
Expectations:			_
$\delta^{44/40}$ Ca	-0.4 to $-0.9%$	<0‰	< -1.6‰
$\delta^{26}$ Mg	< -1‰	> -0.8‰	< -1‰
Mg/Ca	<0.15 mol/mol	<5 mol/mol	$\sim$ 10 mmol/mol
Model fit:			
$\delta^{44/40}$ Ca	-0.4%	-0.6%	-2.1‰
$\delta^{26}$ Mg	-1.8%	-0.2%	-2  to  -1%
Mg/Ca (mmol/mol)	0.025	0.9	20
$\delta^{13}$ C	-11‰	0 to +2‰	-6  to  -3%

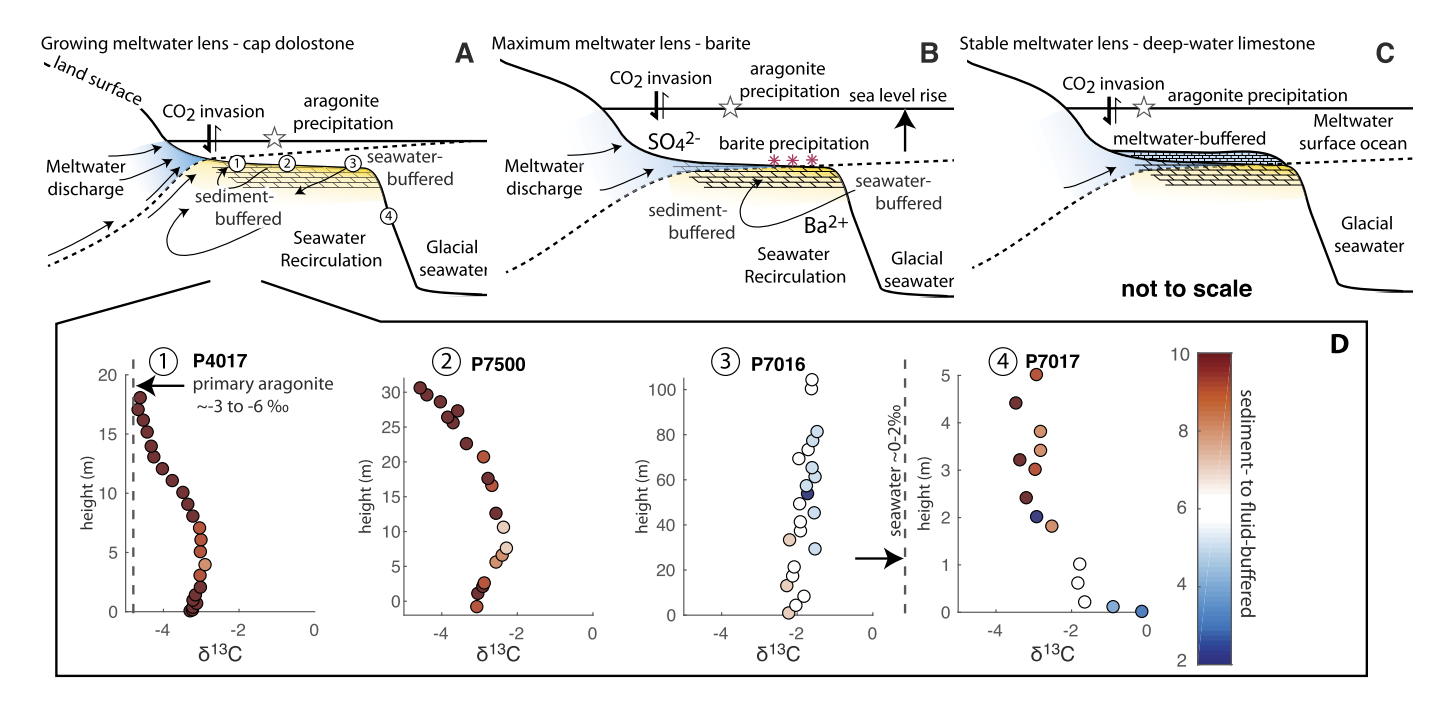


**Fig. 7. Fluid flow during deglaciation.** Schematic representation of fluid circulation in platform sediments during deglaciation. (A) High rates of meltwater discharge from land based ice sheets in the initial stages of deglaciation drives seawater recirculation and dolomitization of primary aragonite in platform environments worldwide. (B) As the meltwater lens reaches its maximum extent, barite precipitates at the interface between meltwater and seawater (dashed line illustrates boundary between meltwater and seawater). (C) While aragonite is continuously precipitating in the surface ocean, dolomitization ceases and is replaced by aragonite neomorphism to calcite as the meltwater lens covers the platform and infiltrates the pore space. (D) Keilberg cap dolostone units from the Congo Craton shown in their relative position across the margin from the inner-most platform environment (P4017) to the foreslope (P7017).  $\delta^{13}$ C values are colored by diagenetic model results of the degree of fluid- versus sediment-buffered dolomitization (on a scale from 0–10 with 10 being the most sediment-buffered), corresponding to the flow path of seawater recirculation through the platform

edge of the platform, establishing convective circulation (Fig. 7). This type of seawater recirculation has been recognized in modern coastal systems (Wilson, 2005), and hypothesized to play an important role in the dolomitization of modern shallow-water carbonate sediments (Vahrenkamp and Swart, 1994).

Seawater recirculation depends on the rate of meltwater discharge at the surface (Cooper et al., 1964; Reilly and Goodman, 1985) and will be most vigorous during ice sheet melting. In addition, seawater recirculation is expected to result in longer fluidflow paths for sites on the inner-most platform and shorter fluidflow paths on the platform edge (Fig. 7). In the context of the cap dolostone, this type of circulation would result in seawaterbuffered dolomites on the platform edge and sediment-buffered dolomites on the inner platform - exactly the spatial pattern observed in the cap dolostone units in Namibia (Fig. 7D). Deeper distal environments will be exposed to less fluid flow because rates of seawater recirculation decline with distance from the freshwaterseawater interface (Cooper et al., 1964; Reilly and Goodman, 1985). As a result, more sediment-buffered carbonates are expected in deeper foreslope settings, consistent with observations from basinal sections in Death Valley (F1340) and Namibia (P7017).

In sections more proximal to land-based ice-sheets, continued meltwater discharge through sediments would result in meteoric-style diagenesis (Fig. 7). This type of diagenesis is consistent with observations from limestones in South Australia (C213) and Kalahari (F817) deposited prior to maximum deglacial flooding. In addition to the lack of dolomite, the observations of very low  $\delta^{26} \rm Mg$  values (down to -4 %) and relatively high  $\delta^{44/40} \rm Ca$  values (up to  $\sim -0.6 \%$ ) in these cap carbonates are consistent with alteration in meltwater-dominated diagenetic fluids. During deglaciation, the growth of the meltwater surface ocean may lead to stratigraphic changes in the style of diagenetic alteration. Sites where diagenesis initially is dominated by circulation of glacial seawater may transition to meltwater-dominated as the thickness of the meltwater surface ocean increases (Fig. 7C). A reduction in seawater

recirculation and a shift to a more meltwater-dominated fluid with time provides an explanation for the stratigraphic transition from a transgressive cap dolostone to a deep-water limestone in multiple sections (e.g., the Maieberg Fm. in Namibia and Hayhook Fm. in Northwest Canada, Fig. 7C). In these limestone units, relatively high  $\delta^{44/40}\text{Ca}$  values (up to  $\sim -0.8\%$ ) and low  $\delta^{26}\text{Mg}$  values (down to  $\sim -3\%$ ) are consistent with alteration in the meltwater lens (e.g., J1132, P4017, Fig. 8).

#### 5.2.4. Barite precipitation

One of the most enigmatic characteristics of the Marinoan cap carbonate sequence is the widespread observation of seafloor barite (BaSO<sub>4</sub>) at the transition between the cap dolostone and the deep-water limestone (e.g., Crockford et al., 2017). This barite hosts unique  $\Delta^{17}$ O anomalies that indicate high  $\text{CO}_2/\text{O}_2$  ratios in the aftermath of the global glaciation and require that  $\text{SO}_4^{2-}$  incorporated into barite was in communication with the atmosphere prior to its incorporation (Bao et al., 2008). We propose that discharge of meltwater provided  $\text{SO}_4^{2-}$  from continental weathering of sulfides (Hoffman et al., 2011; Crockford et al., 2016) while the circulation of anoxic glacial seawater through sediments in the glacial aftermath provided a source of  $\text{Ba}^{2+}$  (Hoffman et al., 2011). This mechanism links the mineralogical transition from dolostone to limestone and the formation of barite to the existence of an interface between the meltwater lens and glacial seawater (Fig. 7B).

## 5.3. Modeling cap carbonate dolomitization and aragonite neomorphism

To test whether the assumptions used to construct our model for cap carbonate deposition and dolomitization are consistent with the observed geochemical variability, we evaluate each dataset using a numerical model of carbonate diagenesis (Ahm et al., 2018). First, the model is used to constrain the composition of the meltwater lens by simulating neomorphism of primary

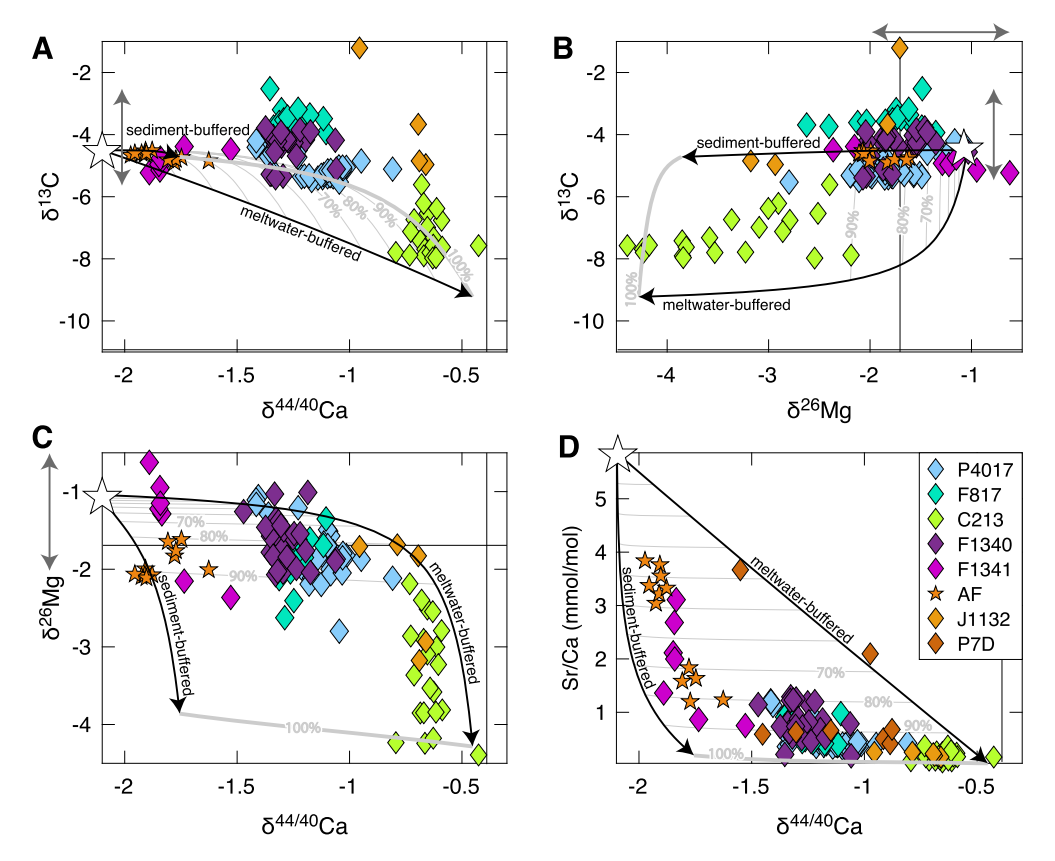


**Fig. 8. Meltwater diagenesis.** Modeling results for neomorphism of primary aragonite (white star) in the meltwater lens (thin black grid lines). The initial composition of aragonite likely varied across the platform (small gray arrow). The two black arrows indicate the two end-member diagenetic pathways for neomorphism in either fully fluid-or sediment-buffered conditions. The gray lines of the model phase-space indicate the degree of neomorphism in the meltwater lens (from 0 to 100%). Model results are compared to measurements from cap limestones from Namibia (blue), Kalahari (cyan), Australia (green), Death Valley (purple/pink), and Northwest Canada (yellow). These measurements span the range between the fluid- and sediment-buffered model trajectories and the primary mineral. (A)  $\delta^{13}$ C versus  $\delta^{44/40}$ Ca values, (B)  $\delta^{13}$ C versus  $\delta^{26}$ Mg values, (C)  $\delta^{26}$ Mg versus  $\delta^{44/40}$ Ca values, and (D) Sr/Ca ratios versus  $\delta^{44/40}$ Ca values. Sample color code and legend correspond to Figs. 1–6.

aragonite in meltwater (based on the concept in Fig. 7). Model results for the meltwater lens are estimated from measurements of  $\delta^{44/40}\text{Ca}$  values,  $\delta^{26}\text{Mg}$  values, and Sr/Ca ratios from cap limestone units. Second, the model is used to constrain the composition of glacial seawater by simulating early marine dolomitization. Model results for glacial seawater are estimated from measurements of  $\delta^{44/40}\text{Ca}$  values,  $\delta^{26}\text{Mg}$  values, and Sr/Ca ratios from the cap dolostone units. Using model results for both dolomitization and neomorphism, we estimate the composition of the primary aragonite and use these constrains to evaluate the origin and variability in  $\delta^{13}\text{C}$  values recorded in cap carbonates worldwide (Table 1).

#### 5.3.1. Aragonite neomorphism in the meltwater lens

A subset of cap carbonate samples from South Australia, Death Valley, Congo, Kalahari, and Northwest Canada are limestone. On the Namibian margin of the Congo craton and in northwestern Canada, deep-water limestones overlie a transgressive cap dolostone unit, but in South Australia, Death Valley, and Kalahari the limestones locally are deposited below the surface of maximum flooding. These limestone units are geochemically distinct from the cap dolostones with low  $\delta^{13}$ C values, high  $\delta^{44/40}$ Ca values, and low  $\delta^{26}$ Mg values (Fig. 8). The most fluid-buffered samples are from South Australia (C213) and record low  $\delta^{26}$ Mg values ( $\sim$  -4‰), relatively high  $\delta^{44/40}$ Ca values ( $\sim$  -0.7‰), and low  $\delta^{13}$ C values ( $\sim$  -7‰, Fig. 3). In contrast, the most sediment-buffered samples are from limestones from a foreslope succession in Death Valley (F1340) that record high  $\delta^{26}$ Mg values ( $\sim$  -1‰), low  $\delta^{44/40}$ Ca values ( $\sim$  -1.9‰), and intermediate  $\delta^{13}$ C values ( $\sim$  -3‰, Fig. 4).

The model fit to the geochemical data from these limestone sections yields a diagenetic fluid with a relatively low  $\delta^{44/40}$ Ca

value ( $\sim$  -0.4%), a very low  $\delta^{26}$ Mg value ( $\sim$  -1.8%), a very low  $\delta^{13}$ C value ( $\sim$  -11%, Fig. 8), and a very low Mg/Ca ratio ( $\sim$ 0.025 mol/mol, Table 1). The range in the geochemical data suggests that the chemistry of the meltwater lens was somewhat variable across different continental margins (Fig. 8), consistent with expectations of the chemistry of a meltwater surface ocean in the aftermath of a global glaciation (section 5.2.1).

#### 5.3.2. Early marine dolomitization

Cap dolostone samples from South Australia, Congo, Kalahari, Death Valley, Northwest Canada, and Arctic Alaska have geochemical signatures consistent with early marine dolomitization by a seawater-like fluid (Fig. 9). The most fluid-buffered samples come from platform margin to upper slope settings on the Congo Craton and in South Australia (C215, P7016, Figs. 2–3) with high  $\delta^{44/40}$ Ca values ( $\sim-0.6\%$ ), low  $\delta^{26}$ Mg values ( $\sim-2.2\%$ ), and high  $\delta^{13}$ C values ( $\sim+2\%$ ). The most sediment-buffered samples come from the innermost platform and deeper foreslope settings of the Congo Craton, and foreslope settings in Death Valley (P4017, P7500, F1340, Figs. 2–4) with low  $\delta^{44/40}$ Ca values ( $\sim-1.5\%$ ), high  $\delta^{26}$ Mg values ( $\sim-1\%$ ), and relatively low  $\delta^{13}$ C values ( $\sim-5\%$ ).

The model fit to the geochemical data from these cap dolostone units (Fig. 9) indicate that the dolomitizing fluid had a  $\delta^{44/40} \text{Ca}$  value of  $\sim$  –0.4‰, a  $\delta^{26} \text{Mg}$  value  $\sim$  –0.2‰, a Mg/Ca ratio of  $\sim$ 0.9 mol/mol, and a  $\delta^{13} \text{C}$  value of  $\sim$ 2‰ (Table 1). However, when excluding a particular section in Australia (C215) with higher  $\delta^{13} \text{C}$  values than observed elsewhere, the model fit to the geochemical data yields a  $\delta^{13} \text{C}$  value of  $\sim$ 0‰ for the dolomitizing fluid. In general, these model estimates are consistent with our expectations for the chemistry of seawater in the wake of a prolonged

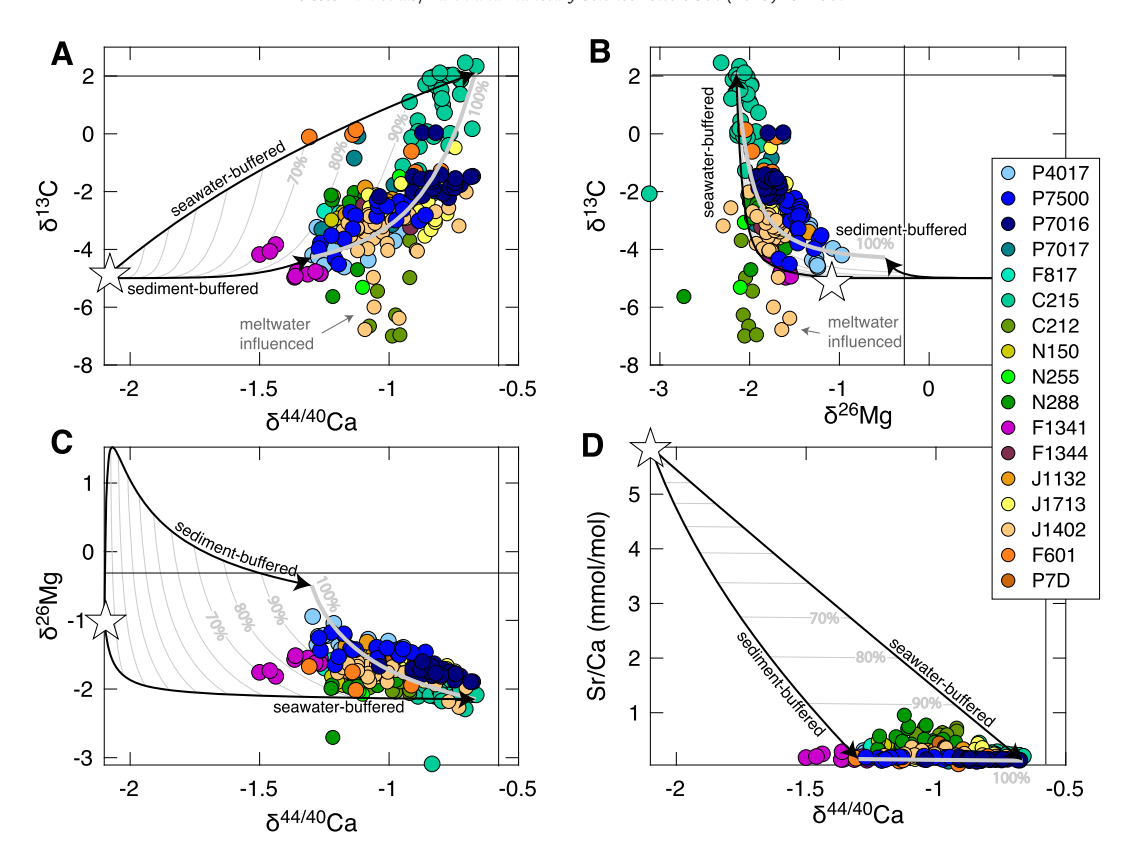


**Fig. 9. Seawater dolomitization.** Modeling results for dolomitization of primary aragonite (white star) in glacial seawater (thin black grid lines). The two black arrows indicate the two end-member diagenetic pathways for dolomitization in either fully fluid- or sediment-buffered conditions. The gray lines on the model phase-space indicate the degree of dolomitization (from 0 to 100%). Grey arrows and text indicate samples that are interpreted to also be influenced by diagenesis in the meltwater surface ocean (see also Fig. 8). Model results are compared to measurements of cap dolostones from Namibia (blue), Australia (green), Death Valley (pink), Northwest Canada (yellow), and Arctic Alaska (orange). These measurements span the range between the fluid- and sediment-buffered model trajectories. (A)  $\delta^{13}$ C versus  $\delta^{44/40}$ Ca values, and (D) Sr/Ca ratios versus  $\delta^{44/40}$ Ca values. Sample color code and legend correspond to Figs. 1–6.

global glaciation where the composition of seawater is set by hydrothermal circulation (section 5.2.2, Hoffman and Schrag, 2002; Jones et al., 2015). The model estimate of relatively high  $\delta^{44/40}$ Ca values of the dolomitizing fluid provide further evidence that the dolomitizing occurred during early marine diagenesis in relatively unaltered seawater as crustal fluids would be expected to have lower  $\delta^{44/40}$ Ca value due to reactions with the wall rock. These model results suggest that the system can be well-represented by a single fluid-buffered end-member for seawater rather than multiple end-members. These results do not imply that smaller scale geochemical variability did not exist during and immediately after deposition of the cap carbonate, but does not support the existence of end-members that are far outside the range of the model phase-space. It is therefore not necessary to change the chemistry of seawater over time to explain the global stratigraphic variability in the geochemistry of basal Ediacaran cap dolostones.

#### 5.3.3. The chemistry of primary aragonite

Model results also can be used to estimate the chemical and isotopic composition of the primary carbonate sediment. The model results outlined above are consistent with primary aragonite with a low  $\delta^{44/40}\text{Ca}$  value ( $\sim -2.1\%$ ) and relatively high  $\delta^{26}\text{Mg}$  values (between  $\sim -1$  and -2%, Table 1, Figs. 8–9). The large range in  $\delta^{26}\text{Mg}$  values in the primary sediment may reflect either a small degree of mixing between Mg-poor meltwater and Mg-rich seawater across the continental margin or small contributions from dolomite in the bulk sample.

The best model fit to the global dataset indicates that the primary aragonite was characterized by  $\delta^{13}C$  values  $\sim -5\%$  with some variability across continents (between  $\sim -6$  and -3%,

Figs. 8–9). This aragonite subsequently was dolomitized in glacial seawater with a  $\delta^{13}$ C value between  $\sim$ 0–2%. Samples that were dolomitized in fluid-buffered settings were reset toward the composition of glacial seawater (e.g., P7016, C215), whereas samples that were dolomitized in more sediment-buffered settings retained some of the chemical signatures of the primary aragonite (e.g., P7500, P4017). Samples that avoided early dolomitization entirely were neomorphosed to low-Mg calcite during diagenesis in the expansive meltwater surface ocean and reflect its low  $\delta^{13}$ C value (e.g., Maieberg Fm. limestones).

#### 5.4. Carbon isotope excursions in cap carbonates

According to our model, the large range in  $\delta^{13}C$  values recorded in cap carbonate deposits worldwide is the consequence of different styles of early diagenesis and fluid flow in platform environments during the glacial aftermath. Model results and measurements of relict aragonite fans suggest that the precursor sediment had low but somewhat variable  $\delta^{13}C$  values (between -3 and -6%, Fig. 8) – a result that is further corroborated by model results of diagenesis in the meltwater surface ocean (down to -11%).

Two mechanisms may explain these low  $\delta^{13}C_{DIC}$  values in the meltwater surface ocean. First, low  $\delta^{13}C_{DIC}$  values are observed in modern coastal systems associated with large fluxes of respired organic matter (Patterson and Walter, 1994). For example, in Florida Bay high rates of submarine groundwater discharge contribute to coastal waters with  $\delta^{13}C_{DIC}$  values down to  $\sim -7\%$ , likely due to the addition of respired organic matter from the Florida Everglades (Patterson and Walter, 1994). To invoke this mechanism and explain the low  $\delta^{13}C_{DIC}$  values in the meltwater lens requires a large

terrestrial biosphere (e.g., Knauth and Kennedy, 2009) or elevated rates of organic carbon oxidation in the underlying sediments.

Alternatively, low  $\delta^{13}C_{DIC}$  values in shallow-water aragonite producing environments may result from kinetic isotope effects due to CO<sub>2</sub> invasion in a poorly-buffered meltwater surface ocean (Baertschi, 1952; Lazar and Erez, 1992). Hydration and/or hydroxvlation of CO<sub>2</sub> is associated with a large kinetic isotope effect (estimates between  $\sim -11$  to -39%, Zeebe and Wolf-Gladrow, 2001) and continued invasion of CO2 into surface waters can result in local  $\delta^{13}C_{DIC}$  values below -10% (Lazar and Erez, 1992). Disequilibrium effects are expressed in modern settings where extremely low  $\delta^{13}C_{DIC}$  values are observed during rapid precipitation of carbonates in high alkalinity waters (e.g., Falk et al., 2016) and/or during high sustained rates of biological productivity in both freshwater (Herczeg and Fairbanks, 1987) and marine environments (Lazar and Erez. 1992). Enhanced nutrient inputs during the intense weathering associated with the post-glacial hothouse (Kunzmann et al., 2013) together with the relatively low buffering capacity of a meltwater surface ocean provide a plausible mechanism to explain the increase in local biological productivity required to produce significant disequilibrium between the meltwater surface ocean and the atmosphere.

Given the important role of photosynthetic microbial mat communities in driving carbon isotopic disequilibrium in modern evaporation pans and sedimentological observations of anomalous 'tubestone' stromatolitic units in the cap carbonate sequence (e.g., Figs. 2, 4, 5; Hoffman et al., 2011), we hypothesize that microbial mats played an important role in driving isotopic disequilibrium in the meltwater surface ocean. The rates of primary production required to drive disequilibrium in both saline microbial mat systems and freshwater lakes are ~30 mmol m<sup>-2</sup> d<sup>-1</sup> (Herczeg and Fairbanks, 1987; Lazar and Erez, 1992), well within the range of estimates for productivity in the modern surface ocean. This hypothesis is not inconsistent with the low organic carbon content in the cap carbonate sequences. While it is generally agreed that microbial mats were likely organic-rich at the sediment-water interface, these same deposits are rarely associated with high concentrations of organic matter in the rock record. In addition, high carbonate precipitation rates may have locally masked organic carbon burial in these sediments. Finally, in addition to providing an explanation for low  $\delta^{13}C_{DIC}$ , productivity-driven disequilibrium may provide insights into the anomalous sedimentary fabrics associated with cap carbonates as disequilibrium in the carbonate system is expected to lead to high degrees of carbonate supersaturation.

According to this hypothesis, the persistence of low  $\delta^{13}C_{DIC}$ values through the cap carbonate sequence above the dolostone units reflect extended periods of disequilibrium between the atmosphere and meltwater surface ocean through the time interval of maximum flooding (Fig. 7C). Periods of disequilibrium were likely driven by algal blooms, resulting in precipitation of aragonite in the less buffered meltwater ocean during times of CO2 invasion. Isotopically depleted crystal fans in deeper-water facies also suggest that these conditions extended to over-deepened shelves and slopes, consistent with the development of a thick meltwater surface ocean (~1 km, Yang et al., 2017) with a duration of  $10^4$ – $10^5$  yr. Due to the decrease in fluid-flow in sediments in deeper-waters, the accumulation of carbonate sediments in deep underfilled basins limited the extent of fluid-buffered alteration and preserved platform top  $\delta^{13}C_{DIC}$  values. These results suggest that the stratigraphic variability of  $\delta^{13}$ C values in the cap carbonate sequence is a product of different styles of diagenesis/dolomitization of primary aragonite. This model explains the regional and stratigraphic variability in terms of mixing between sedimentbuffered neomorphosed aragonite and both sediment- and fluidbuffered dolomite formed from the dolomitization of aragonite with glacial seawater.

Measurements and diagenetic model results of cap dolostone dolomitization suggest that the  $\delta^{13}C_{DIC}$  values of glacial seawater sourced from intermediate water depths was  $\sim$ 0–2% (Fig. 9A). As the  $\delta^{13}C_{DIC}$  value of glacial seawater would depend on the initial  $\delta^{13}C$  of the ocean-atmosphere system, the partitioning of CO<sub>2</sub> between ocean and atmosphere, and temperature-dependent fractionation between the inorganic carbon species,  $\delta^{13}C_{DIC}$  values near 0% are consistent with expectations for glacial seawater (Higgins and Schrag, 2003).

#### 6. Conclusion

- Systematic covariation between Ca and Mg isotope values in more than 20 cap dolostone sections indicate that the dolomite is not a primary precipitate, and instead is the product of secondary early dolomitization of calcium carbonate.
- The low Ca isotope values (below -1.1%) of cap dolomites and the covariation between Ca isotope values and Sr/Ca ratios in the cap limestones indicate that the precursor mineralogy was aragonite.
- Results from diagenetic modeling suggest that primary aragonite was deposited in the meltwater surface ocean with low  $\delta^{13}C_{DIC}$  values (down to  $\sim -11\%$ ).
- δ<sup>13</sup>C values of the meltwater surface ocean were low due to either high rates of organic matter remineralization in glacial groundwater or kinetic isotope effects caused by CO<sub>2</sub> invasion from the atmosphere into the surface ocean. Importantly, these values do not directly reflect secular variations in the DIC.
- Dolomitization of platform sediments is consistent with fluid flow and seawater recirculation during global deglaciation.
- Platform sediments were dolomitized during sea-level rise in glacial seawater with low Mg/Ca ratios ( $\sim$ 0.9), low Ca isotope values ( $\sim$  -0.6%), high Mg isotope values (-0.2%), and  $\delta^{13}C_{DIC}$  values of  $\sim$ 0-2%.

#### Acknowledgements

ASCA acknowledges support from The Carlsberg Foundation. JAH acknowledges support from NSF grant no. IES1410317 and from National Science Foundation OCE CAREER Grant No. 1654571. ASA and CJB acknowledges support from the Danish National Research Foundation (Grant No. DNRF53). We would like to thank Nicolas Slater for assistance in the lab and we thank Clara Blättler, Peter Crockford, and Blake Dyer for insightful discussions. Finally, we thank three anonymous reviewers and the editor for constructive comments that significantly improved this manuscript.

#### Appendix. Supplementary material

Supplementary material related to this article can be found online at https://doi.org/10.1016/j.epsl.2018.10.046.

#### References

Ahm, A-S.C., Bjerrum, C.J., Blättler, C.L., Swart, P.K., Higgins, J.A., 2018. Quantifying early marine diagenesis in shallow-water carbonate sediments. Geochim. Cosmochim. Acta 236, 140–159. https://doi.org/10.1016/j.gca.2018.02.042.

Baertschi, P., 1952. Die fraktionierung der kohlenstoffisotopen bei der absorption von kohlendioxyd. Helv. Chim. Acta 35 (3), 1030–1036. https://doi.org/10.1038/16838830

Bao, H., Lyons, J.R., Zhou, C., 2008. Triple oxygen isotope evidence for elevated CO<sub>2</sub> levels after a Neoproterozoic glaciation. Nature 453, 504–506. https://doi.org/10.1038/nature06959.

Blättler, C.L., Higgins, J.A., 2017. Testing Urey's carbonate-silicate cycle using the calcium isotopic composition of sedimentary carbonates. Earth Planet. Sci. Lett. 479, 241–251. https://doi.org/10.1016/j.epsl.2017.09.033.

- Blättler, C.L., Miller, N.R., Higgins, J.A., 2015. Mg and Ca isotope signatures of authigenic dolomite in siliceous deep-sea sediments. Earth Planet. Sci. Lett. 419, 32–42. https://doi.org/10.1016/j.epsl.2015.03.006.
- Bold, U., Smith, E.F., Rooney, A.D., Bowring, S.A., Buchwaldt, R., Dudás, F.Ö., Ramezani, J., Crowley, J.L., Schrag, D.P., Macdonald, F.A., 2016. Neoproterozoic stratigraphy of the Zavkhan terrane of Mongolia: the backbone for Cryogenian and early Ediacaran chemostratigraphic records. Am. J. Sci. 316, 1–63. https://doi.org/10.2475/01.2016.01.
- Cooper, H.H., Kohout, F.A., Henry, H.R., Glover, R.E., 1964. Sea water in coastal aquifers. U.S. Geol. Surv. Water-Supply Pap. 1613-C, 84.
- Crockford, P.W., Cowie, B.R., Johnston, D.T., Hoffman, P.F., Sugiyama, I., Pellerin, A., Bui, T.H., Hayles, J., Halverson, G.P., Macdonald, F.A., Wing, B.A., 2016. Triple oxygen and multiple sulfur isotope constraints on the evolution of the post-Marinoan sulfur cycle. Earth Planet. Sci. Lett. 435, 74–83. https://doi.org/10.1016/j.epsl.2015.12.017.
- Crockford, P.W., Hodgskiss, M.S., Uhlein, G.J., Caxito, F., Hayles, J.A., Halverson, G.P., 2017. Linking paleocontinents through triple oxygen isotope anomalies. Geology 46 (2), 179–182. https://doi.org/10.1130/G39470.1.
- Fabre, S., Berger, G., Chavagnac, V., Besson, P., 2013. Origin of cap carbonates: an experimental approach. Palaeogeogr. Palaeoclimatol. Palaeoecol. 392, 524–533. https://doi.org/10.1016/j.palaeo.2013.10.006.
- Falk, E.S., Guo, W., Paukert, A.N., Matter, J.M., Mervine, E.M., Kelemen, P.B., 2016. Controls on the stable isotope compositions of travertine from hyperalkaline springs in Oman: insights from clumped isotope measurements. Geochim. Cosmochim. Acta 192, 1–28. https://doi.org/10.1016/j.gca.2016.06.026.
- Fantle, M.S., DePaolo, D.J., 2007. Ca isotopes in carbonate sediment and pore fluid from ODP Site 807A: the Ca<sup>2+</sup>(aq)-calcite equilibrium fractionation factor and calcite recrystallization rates in Pleistocene sediments. Geochim. Cosmochim. Acta 71 (10), 2524–2546. https://doi.org/10.1016/j.gca.2007.03.006.
- Fantle, M.S., Higgins, J., 2014. The effects of diagenesis and dolomitization on Ca and Mg isotopes in marine platform carbonates: implications for the geochemical cycles of Ca and Mg. Geochim. Cosmochim. Acta 142, 458–481. https://doi.org/ 10.1016/j.gca.2014.07.025.
- Gammon, P.R., 2012. An organodiagenetic model for Marinoan-age cap carbonates. Sediment. Geol. 243–244, 17–32. https://doi.org/10.1016/j.sedgeo.2011.12.004.
- Gammon, P.R., McKirdy, D.M., Smith, H.D., 2012. The paragenetic history of a Marinoan cap carbonate. Sediment. Geol. 243–244, 1–16. https://doi.org/10.1016/j.sedgeo.2011.07.004.
- Grotzinger, J.P., Knoll, A.H., 1995. Anomalous carbonate precipitates: is the Precambrian the key to the Permian? Palaios 10 (6), 578–596. https://doi.org/10.2307/3515096.
- Gussone, N., Böhm, F., Eisenhauer, A., Dietzel, M., Heuser, A., Teichert, B.M.A., Reitner, J., Wörheide, G., Dullo, W-C., 2005. Calcium isotope fractionation in calcite and aragonite. Geochim. Cosmochim. Acta 69 (18), 4485–4494. https://doi.org/10.1016/j.gca.2005.06.003.
- Gussone, N., Dietzel, M., 2016. Calcium isotope fractionation during mineral precipitation from aqueous solution. In: Calcium Stable Isotope Geochemistry. In: Advances in Isotope Geochemistry. Springer, Berlin, Heidelberg.
- Herczeg, A.L., Fairbanks, R.G., 1987. Anomalous carbon isotope fractionation between atmospheric CO<sub>2</sub> and dissolved inorganic carbon induced by intense photosynthesis. Geochim. Cosmochim. Acta 51 (4), 895–899. https://doi.org/10.1016/0016-7037(87)90102-5.
- Henderson, G.M., Slowey, N.C., Haddad, G.A., 1999. Fluid flow through carbonate platforms: constraints from <sup>234</sup>U/<sup>238</sup>U and Cl<sup>-</sup> in Bahamas pore-waters. Earth Planet. Sci. Lett. 169 (1–2), 99–111. https://doi.org/10.1016/S0012-821X(99) 00065-5.
- Higgins, J.A., Schrag, D.P., 2003. Aftermath of a snowball Earth. Geochem. Geophys. Geosyst. 4 (3). https://doi.org/10.1029/2002GC000403.
- Higgins, J.A., Schrag, D.P., 2010. Constraining magnesium cycling in marine sediments using magnesium isotopes. Geochim. Cosmochim. Acta 74 (17), 5039–5053. https://doi.org/10.1016/j.gca.2010.05.019.
- Higgins, J.A., Blättler, C.L., Lundstrom, E.A., Santiago-Ramos, D., Akhtar, A., Ahm, A-S.C., Bialik, O., Holmden, C., Bradbury, H., Murray, S.T., Swart, P., 2018. Mineralogy, early marine diagenesis, and the chemistry of shallow water carbonate sediments. Geochim. Cosmochim. Acta 220, 512–534. https://doi.org/10.1016/j.gca.2017.09.046.
- Hoffman, P.F., 2011. Strange bedfellows: glacial diamictite and cap carbonate from the Marinoan (635 Ma) glaciation in Namibia. Sedimentology 58 (1), 57–119. https://doi.org/10.1111/j.1365-3091.2010.01206.x.
- Hoffman, P.F., Macdonald, F.A., 2010. Sheet-crack cements and early regression in Marinoan (635 Ma) cap dolostones: regional benchmarks of vanishing icesheets? Earth Planet. Sci. Lett. 300, 374–384. https://doi.org/10.1016/j.epsl.2010. 10.027.
- Hoffman, P.F., Schrag, D.P., 2002. The Snowball Earth hypothesis: testing the limits of global change. Terra Nova 14 (3), 129–155. https://doi.org/10.1046/j.1365-3121. 2002.00408.x.
- Hoffman, P.F., Kaufman, A.J., Halverson, G.P., Schrag, D.P., 1998. A Neoproterozoic Snowball Earth. Science 281 (5381), 1342–1346. https://doi.org/10.1126/science. 281.5381.1342.
- Hoffman, P.F., Halverson, G.P., Domack, E.W., Husson, J.M., Higgins, J.A., Schrag, D.P., 2007. Are basal Ediacaran (635 Ma) post-glacial "cap dolostones" diachronous?

- Earth Planet. Sci. Lett. 258 (1–2), 114–131. https://doi.org/10.1016/j.epsl.2007.03.
- Hoffman, P.F., Macdonald, F.A., Halverson, G.P., 2011. Chemical sediments associated with Neoproterozoic glaciation: iron formation, cap carbonate, barite and phosphorite. Mem. Geol. Soc. Lond. 36 (1), 67–80. https://doi.org/10.1111/j.1365-3091.2010.01206 x
- Holmden, C., Papanastassiou, D.A., Blanchon, P., Evans, S., 2012.  $δ^{44/40}$ Ca variability in shallow water carbonates and the impact of submarine groundwater discharge on Ca-cycling in marine environments. Geochim. Cosmochim. Acta 83, 179–194. https://doi.org/10.1016/j.gca.2011.12.031.
- Husson, J.M., Higgins, J.A., Maloof, A.C., Schoene, B., 2015. Ca and Mg isotope constraints on the origin of Earth's deepest C excursion. Geochim. Cosmochim. Acta 160, 243–266. https://doi.org/10.1016/j.gca.2015.03.012.
- Jacobson, A.D., Holmden, C., 2008. δ<sup>44</sup>Ca evolution in a carbonate aquifer and its bearing on the equilibrium isotope fractionation factor for calcite. Earth Planet. Sci. Lett. 270 (3–4), 349–353. https://doi.org/10.1016/j.epsl.2008.03.039.
- Jacobson, A.D., Zhang, Z., Lundstrom, C., Huang, F., 2010. Behavior of Mg isotopes during dedolomitization in the Madison aquifer, South Dakota. Earth Planet. Sci. Lett. 297 (3), 446–452. https://doi.org/10.1016/j.epsl.2010.06.038.
- Jiang, G., Kennedy, M.J., Christie-Blick, N., 2003. Stable isotopic evidence for methane seeps in Neoproterozoic postglacial cap carbonates. Nature 426, 822–826. https://doi.org/10.1038/nature02201.
- Jones, C., Nomosatryo, S., Crowe, S.A., Bjerrum, C.J., Canfield, D.E., 2015. Iron oxides, divalent cations, silica, and the early earth phosphorus crisis. Geology 43 (2), 135–138. https://doi.org/10.1130/G36044.1.
- Kasemann, S.A., Hawkesworth, C.J., Prave, A.R., Fallick, A.E., Pearson, P.N., 2005. Boron and calcium isotope composition in Neoproterozoic carbonate rocks from Namibia: evidence for extreme environmental change. Earth Planet. Sci. Lett. 231 (1–2), 73–86. https://doi.org/10.1016/j.epsl.2004.12.006.
- Kasemann, S.A., Pogge von Strandmann, P.A.E., Prave, A.R., Fallick, A.E., Elliott, T., Hoffmann, K.-H., 2014. Continental weathering following a Cryogenian glaciation: evidence from calcium and magnesium isotopes. Earth Planet. Sci. Lett. 396, 66–77. https://doi.org/10.1016/j.epsl.2014.03.048.
- Kennedy, M.J., 1996. Stratigraphy, sedimentology, and isotopic geochemistry of Australian Neoproterozoic postglacial cap dolostones; deglaciation,  $\delta^{13}C$  excursions, and carbonate precipitation. J. Sediment. Res. 66 (6), 1050–1064. https://doi.org/10.2110/jsr.66.1050.
- Kennedy, M.J., Christie-Blick, N., Sohl, L.E., 2001. Are Proterozoic cap carbonates and isotopic excursions a record of gas hydrate destabilization following Earth's coldest intervals? Geology 29 (5), 443–446. https://doi.org/10.1130/0091-7613(2001)029<0443:APCCAI>2.0.CO;2.
- Kirschvink, J.L., 1992. Late Proterozoic low-latitude global glaciation: the Snowball Earth. In: The Proterozoic Biosphere: A Multidisciplinary Study. Cambridge University Press.
- Knauth, L.P., Kennedy, M.J., 2009. The late Precambrian greening of the Earth. Nature 460 (7256), 728–732. https://doi.org/10.1038/nature08213.
- Knoll, A.H., Walter, M., Narbonne, G.M., Christie-Blick, N., 2006. The Ediacaran Period: a new addition to the geologic time scale. Lethaia 39 (1), 13–30. https://doi.org/10.1080/00241160500409223.
- Komar, N., Zeebe, R.E., 2016. Calcium and calcium isotope changes during carbon cycle perturbations at the end-Permian. Paleoceanography 31 (1), 115–130. https://doi.org/10.1002/2015PA002834.
- Kunzmann, M., Halverson, G.P., Sossi, P.A., Raub, T.D., Payne, J.L., Kirby, J., 2013. Zn isotope evidence for immediate resumption of primary productivity after snowball Earth. Geology 41 (1), 27–30. https://doi.org/10.1130/G33422.1.
- Lazar, B., Erez, J., 1992. Carbon geochemistry of marine-derived brines: I. <sup>13</sup>C depletions due to intense photosynthesis. Geochim. Cosmochim. Acta 56 (1), 335–345. https://doi.org/10.1016/0016-7037(92)90137-8.
- Liu, C., Wang, Z., Raub, T.D., Macdonald, F.A., Evans, D.A.D., 2014. Neoproterozoic cap-dolostone deposition in stratified glacial meltwater plume. Earth Planet. Sci. Lett. 404, 22–32. https://doi.org/10.1016/j.csr.2013.08.007.
- Liu, C., Wang, Z., Macdonald, F.A., 2018. Sr and Mg isotope geochemistry of the basal Ediacaran cap limestone sequence of Mongolia: implications for carbonate diagenesis, mixing of glacial meltwater, and seawater chemistry in the aftermath of Snowball Earth. Chem. Geol. 491, 1–13. https://doi.org/10.1016/j.chemgeo.2018. 05.008
- Macdonald, F.A., McClelland, W.C., Schrag, D.P., Macdonald, W.P., 2009. Neoproterozoic glaciation on a carbonate platform margin in Arctic Alaska and the origin of the North Slope subterrane. Geol. Soc. Am. Bull. 121 (3/4), 448–473. https://doi.org/10.1130/B26401.1.
- Macdonald, F.A., Prave, A.R., Petterson, R., Smith, E.F., Pruss, S.B., Oates, K., Waechter, F., Trotzuk, D., Fallick, A.E., 2013a. The Laurentian record of Neoproterozoic glaciation, tectonism, and eukaryotic evolution in Death Valley, California. Geol. Soc. Am. Bull. 125 (7–8), 1203–1223. https://doi.org/10.1130/B30789.1.
- Macdonald, F.A., Strauss, J.V., Sperling, E.A., Halverson, G.P., Narbonne, G.M., Johnston, D.T., Kunzmann, M., Schrag, D.P., Higgins, J.A., 2013b. The stratigraphic relationship between the Shuram carbon isotope excursion, the oxygenation of Neoproterozoic oceans, and the first appearance of the Ediacara biota and bilaterian trace fossils in northwestern Canada. Chem. Geol. 362, 250–272. https://dx.doi.org/10.1016/j.chemgeo.2013.05.032.

- Patterson, W.P., Walter, L.M., 1994. Depletion of <sup>13</sup>C in seawater CO<sub>2</sub> on modern carbonate platforms: significance for the carbon isotopic record of carbonates. Geology 22 (10), 885–888. https://doi.org/10.1130/0091-7613(1994)022<0885: DOCISC>2.3.CO;2.
- Raub, T.D., 2008. Prolonged deglaciation of "Snowball Earth" (Order No. 3317273).

  Available from ProQuest Dissertations and Theses Global; SciTech Premium Collection (304390388). https://search.proquest.com/docview/304390388? accountid=13314.
- Reilly, T.E., Goodman, A.S., 1985. Quantitative analysis of saltwater-freshwater relationships in groundwater systems a historical perspective. J. Hydrol. 80 (1), 125–160. https://doi.org/10.1016/0022-1694(85)90078-2.
- Rose, C.V., Maloof, A.C., 2010. Testing models for post-glacial 'cap dolostone' deposition: Nuccaleena Formation, South Australia. Earth Planet. Sci. Lett. 296 (3–4), 165–180. https://doi.org/10.1016/j.epsl.2010.03.031.
- Shields, G.A., 2005. Neoproterozoic cap carbonates: a critical appraisal of existing models and the plumeworld hypothesis. Terra Nova 17 (4), 299–310. https://doi.org/10.1111/j.1365-3121.2005.00638.x.
- Silva-Tamayo, J.C., Nägler, T.F., Sial, A.N., Nogueira, A., Kyser, K., Riccomini, C., James, N.P., Narbonne, G.M., Villa, I.M., 2010. Global perturbation of the marine Ca isotopic composition in the aftermath of the Marinoan global glaciation. Precambrian Res. 182 (4), 373–381. https://doi.org/10.1016/j.precamres.2010.06.015.
- Tang, J., Dietzel, M., Böhm, F., Köhler, S., Eisenhauer, A., 2008. Sr<sup>2+</sup>/Ca<sup>2+</sup> and <sup>44</sup>Ca/<sup>40</sup>Ca fractionation during inorganic calcite formation: II. Ca isotopes. Geochim. Cosmochim. Acta 72 (15), 3733–3745. https://doi.org/10.1016/j.gca. 2008.05.033

- Tipper, E.T., Galy, A., Gaillardet, J., Bickle, M.J., Elderfield, H., Carder, E.A., 2006. The magnesium isotope budget of the modern ocean: constraints from riverine magnesium isotope ratios. Earth Planet. Sci. Lett. 250 (1–2), 241–253. https://doi.org/10.1016/j.epsl.2006.07.037.
- Trindade, R.I.F., Font, E., D'Agrella-Filho, M.S., Nogueira, A.C.R., Riccomini, C., 2003. Low-latitude and multiple geomagnetic reversals in the Neoproterozoic Puga cap carbonate, Amazon craton. Terra Nova 15 (6), 441–446. https://doi.org/10.1046/j.1365-3121.2003.00510.x.
- Vahrenkamp, V.C., Swart, P.K., 1994. Late Cenozoic dolomites of the Bahamas: metastable analogues for the genesis of ancient platform dolomites. In: Dolomites. Blackwell Publishing Ltd., pp. 133–153.
- Wang, Z., Hu, P., Gaetani, G., Liu, C., Saenger, C., Cohen, A., Hart, S., 2013. Experimental calibration of Mg isotope fractionation between aragonite and seawater. Geochim. Cosmochim. Acta 102, 113–123. https://doi.org/10.1016/j.gca.2012.10.022.
- Wilson, A.M., 2005. Fresh and saline groundwater discharge to the ocean: a regional perspective. Water Resour. Res. 41 (2). https://doi.org/10.1029/2004WR003399.
- Yang, J., Jansen, M.F., Macdonald, F.A., Abbot, D.S., 2017. Persistence of a freshwater surface ocean after a snowball Earth. Geology 45 (7), 615–618.
- Zeebe, R.E., Wolf-Gladrow, D., 2001. CO<sub>2</sub> in Seawater: Equilibrium, Kinetics, Isotopes. Elsevier Oceanography Series, vol. 65.